Investigation of XBeach Cross-Shore Capacity Under Fixed Model Parameters

Dawit Tilahun Seyoum

Submitted in fulfillment of the academic requirement for the degree of

Master of Science in Civil Engineering

in the

Civil Engineering Programme

University of KwaZulu-Natal

Durban

2020

Supervisors: Professor D. D. Stretch and Dr J.J Pringle

DECLARATION

I *Dawit Tilahun Seyoum* declare that

- This work was done wholly or mainly while in candidature for a Master of Science in Civil Engineering at the University of KwaZulu-Natal.
- Where any part of this document has previously been submitted for a degree or any other qualification at this University or any other institution, this has been clearly stated.
- Where I have consulted the published work of others, this is always clearly attributed.
- Where I have quoted from the work of others, the source is always given. With the exception of such quotations, this document is entirely my own work.
- I have acknowledged all main sources of help.

Signed and Date:

Mr. D.T Seyoum

As the candidate's supervisor I agree to the submission of this dissertation.

Signed and Date:

Prof. Derek D. Stretch

Signed and Date:

Dr. Justin J. Pringle

ACKNOWLEDGEMENTS

I would firstly like to thank my supervisors Prof. Derek Stretch and Dr. Justin Pringle of the School of Civil Engineering and the Built Environment at University of KwaZulu-Natal. The door to Prof. Derek Stretch and Dr. Justin Pringle office was always open whenever I ran into a trouble or had a question about my research or writing. I highly appreciate their push.

I would also like to thank the eThekwini municipality for providing me with wave buoy data for this research project.

I must express my very profound gratitude to my parents and to my girlfriend for providing me with unfailing support and continuous encouragement throughout my years of study and the constant edits they have helped me with through the process of researching and writing this thesis. This accomplishment would not have been possible without them. Thank you.

Finally, but most importantly, I would like to give all glory to Yeshua/ Elohim, all mighty God for gracing me with His strength, seeds of hope, and dreams that drive me to persevere through difficult times.

ABSTRACT

An accurate, computationally efficient shoreline model is fundamental to understanding long term shoreline behaviour. Currently, one-line models can be used to perform this but are limited to either cross-shore or alongshore changes only. A simple, more robust model could be developed based on volumetric beach profile changes. However, this requires large empirical datasets to explore the relationships between wave and shoreline variables. In instances where such data is not available, process-based models such as XBeach are an attractive solution. Therefore, it is important to explore the ability of processes-based models such as XBeach to accurately predict shoreline changes under varying wave conditions. In this study two wave conditions associated with erosion (H_s =3m) and accretion (H_s =1m) were used to evaluate the performance of XBeach to accurately predict shoreline changes. The east coast of South Africa was used as a case study site. The coastal areas of South Africa are known for their high energy wave climate resulting in a dynamic shoreline, with significant onshore and offshore sediment transportation. The effects of wave non-linearities on sediment transport was estimated using XBeach's built-in wave asymmetry and the skewness calibrating factors. The sensitivity of sediment transport to these parameters was investigated by running 180, 1D wave flume simulations. The 180 simulations were formulated by varying the wave asymmetry and skewness calibrating factors, sediment transport models, and approaching wave conditions. The results showed that increasing the magnitude of the calibrating factors increased onshore sediment transport. This was attributed to an increase in the advection velocity in the onshore direction. The investigations on the model capacity showed that the wave asymmetry and skewness related parameters control the cross-shore sediment movement direction. It was found that a single set of model input parameters were not able to produce both onshore sediment transport during low energy wave conditions and offshore sediment transport during high energy wave conditions. This study

demonstrated that calibrating factors should depend on incoming wave energy. Currently, they are not implemented like this in XBeach.

TABLE OF CONTENTS

LIST OF FIGURES

LIST OF TABLES

CHAPTER 1: INTRODUCTION

The chapter contains the motivation of the research, aims and objectives, and the outline of this dissertation.

1.1 Background and Motivation

In regions with limited shoreline observations, coastal engineers rely on numerical models to explore the shoreline changes that are expected to occur as a result of observed and forecasted wave conditions. Accurate simulations of shoreline changes are essential to improve coastal engineering designs. In such regions, where there is limited shoreline observations, the numerical simulations should simulate both accretion and erosion as a function of the approaching wave energy. High energy waves drive offshore sediment transport in coastal areas throughout the world (Dean & Dalrymple, 2004; Corbella & Stretch, 2012b; Jara *et al*., 2015).

Cross-shore sediment transport occurs over a shorter time scale in comparison to alongshore sediment transport. Therefore, during storm events, the cross-shore sediment transport is more dominant and results in significant changes to shoreline positions and beach profile shape. Figure 1.1 shows the result of cross-shore sediment transport under high energy wave conditions. These changes have a negative impact on both the infrastructure and economy of the affected coastal area. Although, coastal areas are susceptible to storm wave conditions, the implementation of hard and soft engineering solutions, such as breakwaters and geotextile sand-filled containers, can mitigate the damages that occur during the large wave events. The soft engineering solutions such as Geotextile Sand-filled Containers (GSCs) are usually preferred because they are not permanent structures and have minimal effects on coastal environments (Corbella & Stretch, 2012a). GSCs are used as artificial dunes (i.e. where they are covered by sand and vegetation). Allan & Komar (2003) reported that this method

managed to withstand extreme wave conditions from 1999 to 2002 that would have eroded the dune, resulting in the shoreline recession and beach sand volume loss. Hence, the GSC revetment is to be placed on parts of the coastline where the beach experiences the most concentrated wave energy during extreme wave conditions.

Figure 1.1. 2007 Storm damage to (a) Ballito Bay and (b) Umkomaas (Mather, 2012)

Understanding the volumetric sand changes of a beach as a function of the approaching wave energy is essential to predicting the potential damages that might occur, and manage coastlines effectively. Volumetric sediment transport models should reliably predict the volumetric change expected as a function of the change in mean wave energy experienced as a result of the changing seasons. This will enable a better understanding of the shoreline behaviour in response to changes in the beach sand volume and changing wave energies. Accurate and realistic simulation of the shoreline and volumetric changes as a function of the approaching wave energy will allow coastal engineers to make informed decisions, which affect the design of coastal structures, such as revetments as the design is dependent on the shoreline position.

Seasonal changes are associated with a change in the net wave energy that the beach experiences, thus resulting in the formation and migration of sand bars, as shown in Figure 1.2. The net sediment transport rate and direction are directly related to the net energy (Türker & Kabdaşlı, 2007). During seasons with high energy wave conditions, off-shore bars form and move away from the beach (Dean & Dalrymple, 2004). However, during seasons with low

wave energy the off-shore bars migrate back towards the shore.

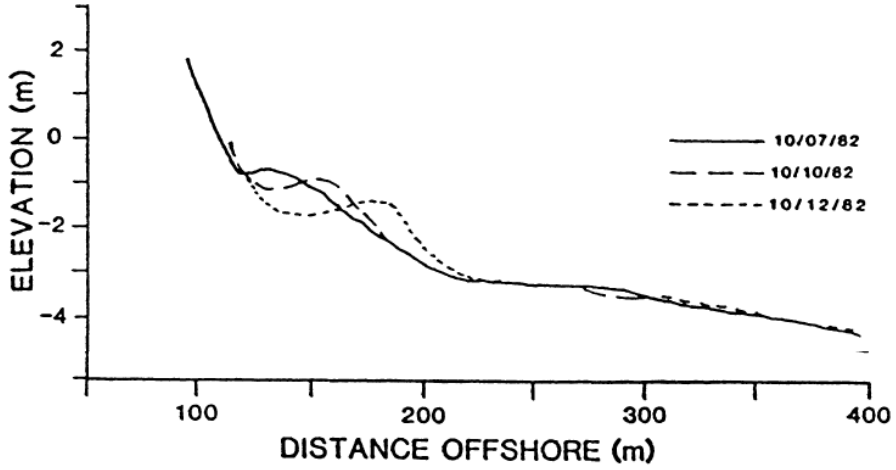

Figure 1.2. The description of the formation and migration of sand bars as a result of a high energy wave condition, measured at Duck-82 (Holman & Sallenger Jr, 1993)

Modelling shoreline responses to storm waves assist in predicting the vulnerability of the coastal areas for expected future events. The available shoreline change data can be used to measure changes in the coastal areas. Although the available data doesn't span years, the use of realistic and accurate models to simulate the shoreline changes enables the exploration of shoreline responses to future events. Furthermore, it aids in selecting the most suitable engineering solutions to mitigate future problems, such as shoreline recessions and beach volume loss (Pereira et al., 2013, Jara et al., 2015). The various types of models used for predicting coastal processes have both advantages and disadvantages. While process-based models attempt to resolve the physics of sediment movement and their driving forces, the disadvantages of such models include the need for extensive input data in addition to requiring long simulation times. It is, therefore, imperative to develop a simple model that is computationally efficient in terms of processing time, computer memory requirement, and accuracy of the outcome. The development of such models will assist in predicting shoreline change at both short and long term cases. A recent example of such a model is the dynamic equilibrium model (DEM) developed by Jara *et al.* (2015). It is based on the perturbation of the shoreline as a result of the incoming wave energy. Pringle (2015) used the DEM to

simulate the shoreline changes for 16 years, as shown in Figure 1.3. The simulated shoreline position shows both accretion due to low energy wave conditions and erosion due to high energy wave conditions. The constraints of DEM are yet to be validated with diverse beach characteristics, which requires initial shoreline change and wave climate data.

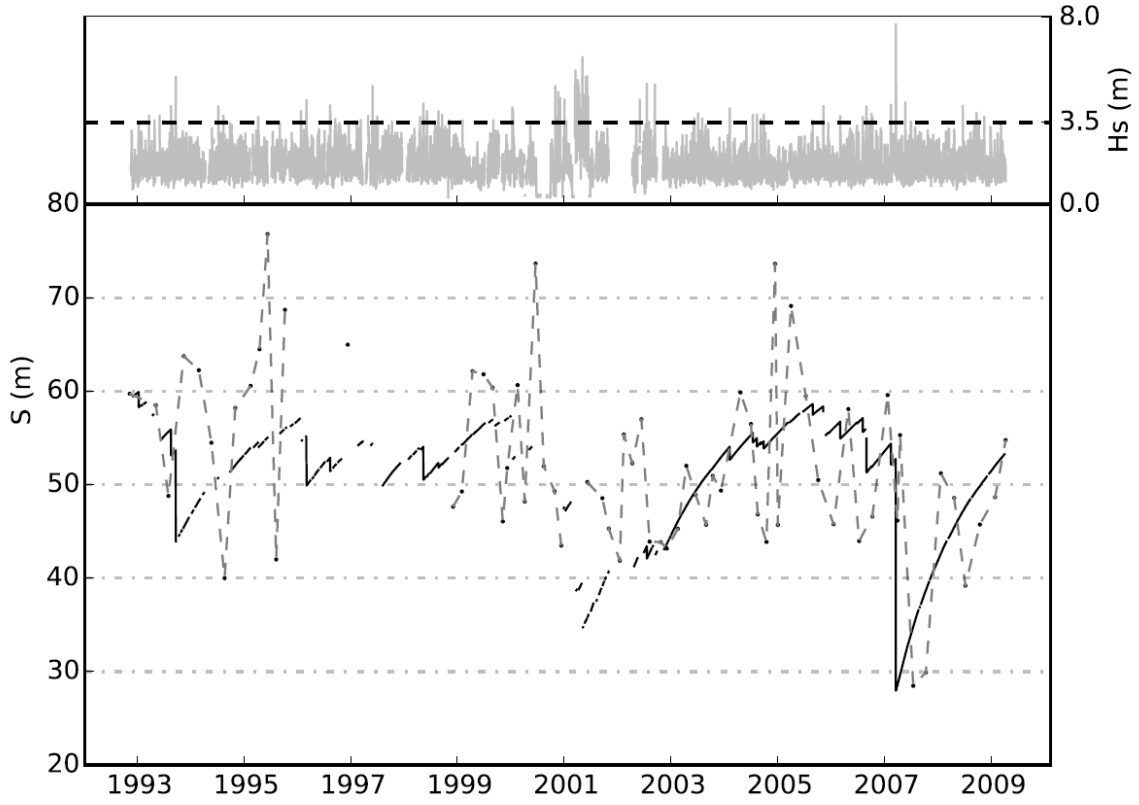

Figure 1.3. 16-year shoreline change simulation using the DEM and wave buoy data (Pringle, 2015). The simulated shoreline position, as shown by solid black-line. Measured shoreline position data is shown by dashed black line.

XBeach is a good example of a process-based model that predicts shoreline change due to wave forces (Roelvink *et al.*, 2009, 2010). The advection velocity used in the advection-diffusion model accounts for the wave non-linearities. This velocity is a function of wave skewness, asymmetry, orbital velocity, and their relative importance as specified by calibrating factors. It is essential to understand the ability of such models to simulate accurate sediment transport in the cross-shore and alongshore directions. Process-based models can be used

to generate the hydrodynamic and morphological data to be used for the development of simplified volumetric models.

1.2 Problem Statement

South African coastal areas experience seasonal and energetic wave climates that result in a dynamic shoreline. Due to seasonal changes, the wave climate varies from high energy to low energy. Seasons with relatively high wave energies contribute to the formation of a nearshore bar and diminishing beach width. In contrast, seasons with lower wave energies result in the creation of dunes and an increase in the beach width. The experienced wave energies drive sediment transport at a range of time scales and result in a highly irregular shoreline. Cross-shore sediment transportation occurs at a short time scale, whereas alongshore sediment transportation occurs over longer time scales. During high energy wave conditions, the rate of cross-shore sediment transportation is dominant over alongshore sediment transportation. The imbalance in the magnitude of sediment transport in the cross-shore and alongshore direction results in a noticeable impact on the shoreline (i.e., the erosion of dunes and beach face leading to shoreline recession). Like South African coastal areas, coastal areas around the world are susceptible to high energy wave conditions and experience the same problem of shoreline recession (Dean & Dalrymple, 2004; Lemos *et al.*, 2017).

Simulating shoreline changes and the resulting volume change of the beach face, due to the net cross-shore sediment transport, can assist coastal engineers in the design of coastal structures. The existing process-based models (i.e. XBeach, Delft3D.) are computationally demanding and are therefore not efficient for long term simulations. Long term simulations ran using a simple parameterization of beach sand volume changes as a result of beach morphology and sediment characteristics can have low computational costs. An already existing long term wave energy data-set can be used to run long term simulations at low computational cost.

The development of the parametrized volumetric model is reliant on a large data-set of beach volume change, and shoreline position. Some data is available as a form of beach surveys. However, long term data is necessary to parametrize volumetric sediment transport. Process-based model such as XBeach can be used to generate the data required for the development of the parametrized volumetric sediment transport model. Hence, the feasibility of XBeach to generate the necessary data for the development of the parameterized volumetric model.

1.3 Research Question

Can process-based models such as XBeach predict both beach erosion and accretion (beach recovery) for high and low wave conditions?

1.4 Aim

This study aims to evaluate the ability of XBeach to accurately predict cross-shore sediment transport under various wave conditions.

1.5 Objectives

The specific objectives of this study are:

- To use the Durban wave data in order to select wave conditions used to test for accretion and erosion cases.
- To investigate the sensitivity of flow velocity and advection velocity as a function of the tested parameters.
- To investigate the ability of XBeach to predict both accretion and erosion cases, using the available sediment transport models, with fixed model parameters.
- To investigate the sensitivity of sediment transport modules to the varying wave asymmetry calibrating factors.

1.6 Methodological Approaches

The methodological approaches of this study are to:

- review beach survey reports to understand the features of the sediment characteristics in the KwaZulu-Natal coastal area.
- select the cross-shore grid spacing as a function of cross-shore bed change.
- set up a 1D XBeach model and test the two wave conditions selected in order to investigate the model's ability to simulate accretion and erosion for low and high energy wave conditions respectively, with fixed model parameters.
- identify parameters used to calibrate sediment transport in XBeach, and investigate the sensitivity of sediment transport and advection velocity to these parameters.

1.7 Thesis Structure

- Chapter 2 is a literature review of nearshore hydrodynamics resulting from ocean waves, and the drivers of sediment transport. The review also includes a review of sediment transport models.
- Chapter 3 discusses the model set up processes, and methods used to test the cross-shore capacity of XBeach.
- Chapter 4 displays the results obtained from the test conducted on XBeach cross-shore capacity. Furthermore, the sensitivity of the sediment transport models to wave asymmetry and skewness calibrating factors are analyzed and presented.
- Chapter 5 presents the conclusions drawn from the XBeach cross-shore sediment transport capability study.

CHAPTER 2: LITERATURE REVIEW

This chapter reviews how wave formation and transformation effects near-shore sediment transport and how these processes are parameterised in process-based models.

2.1 Wave Formation and Grouping

Waves are variations in the water surface at a certain location due to the wind and atmospheric pressure changes (Jeffreys, 1925; Bosboom & Stive, 2012). Airy (1845) describes the water level displacement due to the oscillation of the waves that propagate along the ocean using

$$\eta(x,t) = \frac{H}{2} cos(kx - \sigma t) \tag{2.1}$$

where H is wave height, k is wavenumber ($k = \frac{2\pi}{L}$), x is the direction of wave propagation, σ is the angular frequency ($\sigma = \frac{2\pi}{T}$), L is the wavelength, T is wave period, and t is time.

Equation 2.1 is otherwise known as linear (Airy) wave theory (Airy, 1845). Linear (Airy) wave theory is only applicable if the wavelength is significantly higher than the wave height ($L > H$), this condition is met in deepwater waves. Hence, Linear (Airy) wave theory can simulate deepwater waves well (Airy, 1845). However, it becomes unstable in shallow water due to wave non-linearities .

Once the waves have formed, they travel long distances from the point of generation to reach the coastal areas. As these waves travel towards a coastline; they accelerate, increase in wavelength, and in deepwater the wave shape becomes regular (Bosboom & Stive, 2012). These waves are called swells (Bosboom & Stive, 2012). Waves that are short, random, irregular and generated by the wind are called the sea. Phenomena such as white-capping

and the formation of currents are a part of dissipation processes that assist in filtering out short waves (Bosboom & Stive, 2012).

Propagating wave groups result in sediment transport in the direction of propagation. An experimental study of the relationship between sediment characteristics and sediment transport under wave groups showed that there is a higher transport rate in the direction of the wave group propagation (Sato, 1993). Yu *et al*. (2010) showed that increasing and decreasing the wave group period influences the location of wave breaking in addition to the change in the shoreline position.

2.2 Wave Transformation

As waves approach the shore, they interact with the seabed and begin to shoal when $H \leq h/2$, where H is the wave height, and h is water depth. This process consists of a change in wave height, wavelength and wave group speed. During the shoaling process, the wave height increases, while the wavelength and wave group speed decrease (Deigaard *et al*., 1992). During the shoaling process, the asymmetry and skewness of the waves are affected due to the changes in the wavelength and velocity (Bosboom & Stive, 2012). Waves with a wave height to wavelength ratio of less than 0.14 are linear waves whilst waves with a wave height to wavelength ratio of greater than 0.14 are non-linear waves (Schwartz & Fenton, 1982). The changes to the wavelength and wave velocity are the driving factors resulting in wave non-linearities. Furthermore, the change in water depth as waves approach the shore amplifies this process, as waves are limited to the depth of water they travel in (Bosboom & Stive, 2012). The changes in the wave asymmetry and skewness are reflected in the orbital velocity (Rocha *et al*., 2013). Wave asymmetry and skewness are the contributing factors to offshore transport during storm events, which results in a significant shoreline recession over a short period (Deigaard *et al*., 1992; Bosboom & Stive, 2012). Therefore, understanding their contribution to cross-shore sediment transport in process-based models is essential to

producing realistic sediment transport rates in simulations. Wave asymmetry and skewness change due to shoaling, as can be described by Figure 2.1a and 2.1b.

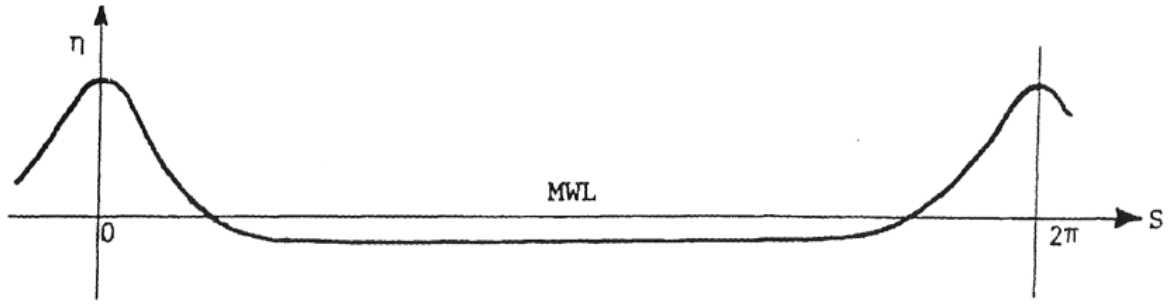

(a)

(b)

Figure 2.1. a) Peaked crest and flattened trough making up a skewed wave, b) A steep wave face that is peaked forward (Battjes, 2001).

2.2.1 Wave Breaking

As waves approach the near-shore zone, they shoal and their wave steepness increases. There is a physical limit to this steepness. The wave height will increase to infinity without this limit (Mlche, 1944). Wave steepness is a ratio of wave height and wavelength. The wave steepness criteria are different for deepwater and shallow water. The wave steepness in deepwater is a function of deepwater wave height and wavelength (Bosboom & Stive, 2012). The maximum wave steepness (critical wave steepness) before wave breaking in deepwater is 0.142 ($\approx$ 1/7). However, in shallow water, the critical wave steepness is a function of water depth and shallow water wavelength (Bosboom & Stive, 2012). The shoaling wave starts to break as it

can no longer resist shear, and the wave steepness exceeds the critical steepness. Figure 2.2 shows the critical crest angle (Bosboom & Stive, 2012). The approximated maximum wave steepness in deep and shallow water is given as

$$\left[\frac{H_0}{L_0}\right]_{max} = 0.142 \approx \frac{1}{7} \tag{2.2}$$

$$\left[\frac{H}{L}\right]_{max} = 0.142\frac{2\pi h}{L} \tag{2.3}$$

where H_0 is deepwater wave height, L_0 is deepwater wavelength, H is shallow water wave height, L is shallow water wavelength, and h is local water depth.

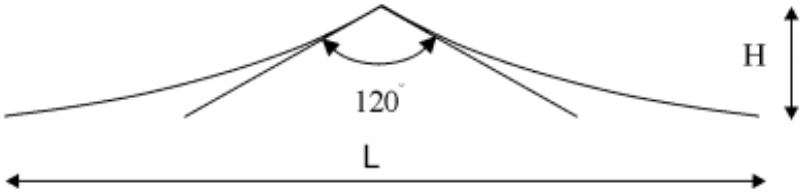

Figure 2.2. The maximum wave crest angle (Bosboom & Stive, 2012). H is wave height, and L is the wavelength

According to Battjes (1975),Bosboom & Stive (2012), and Clavero *et al*. (2018) the type of breaking depends on the change in the deepwater wave characteristics and bed slope. The Iribarren number is a dimensionless parameter used to model several effects of breaking (Battjes, 1975). The Iribarren number is calculated using the combination of the deepwater wave characteristics and bed slope as given by

$$\xi = \frac{tan\alpha}{\sqrt{\frac{H_0}{L_0}}} \tag{2.4}$$

where ξ is Iribarren number, α is beach slope, H_0 is Deep water wave height, and L_0 is deepwater wave length. Figure 2.3 shows examples of different Iribarren numbers and effect on wave breaking. Table 2.1 shows the type of breaker relative to the wave steepness and beach slope angle. This shows that the wave steepness is inversely proportional to the beach slope angle.

Table 2.1 Beach slope angle and wave steepness of the different breaker types as described by the Iribarren parameter.

Breakers	**Wave Steepness**	**Slope angle**
Surging	lowest	Highest
Collapsing	.	.
Plunging	.	.
Spilling	Highest	Lowest

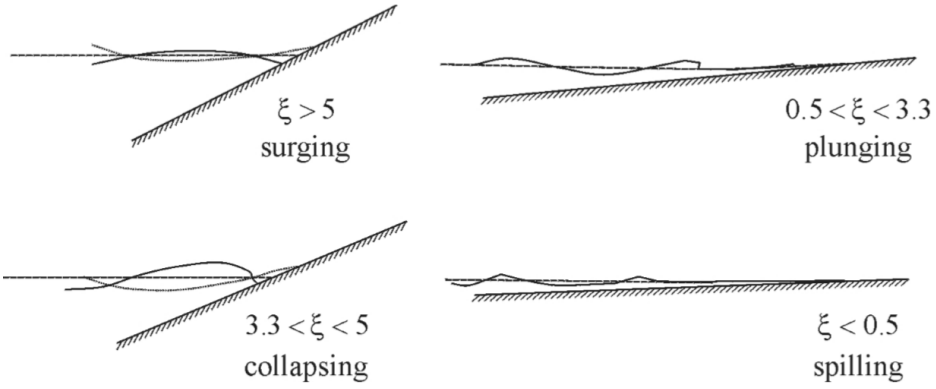

Figure 2.3. The different types of breaking based on the Iribarren parameter (Bosboom & Stive, 2012).

2.2.2 Non-linear Effects in Shoaling Waves

The movement of a water particle in deep water due to a propagating wave is circular (Bosboom & Stive, 2012). This circular motion becomes more elliptic as the propagating wave approaches the coast and the water depth decreases (Ruessink *et al.*, 2012). The water particles move towards the shore below the crest and away from the shore beneath the trough. In deep water, a water depth to wavelength ratio that results in a circular motion of the water particle is, given as

$$h/L > 0.5 \tag{2.5}$$

where h is the water depth and L is the wavelength. However in shallow water ($h/L < 0.5$), the paths become elliptical (Masselink *et al.*, 2014; Sorensen, 2005). In the swash zone, the orbital motion of the water particles start to become more ellipsoid. Figure 2.4 shows the evolution of the shape of the path that the particles follow due to the orbital velocity in deep

and shallow water. The parallel back and forth motion of the water particle found in the shallow waters is known as being oscillatory (Van Rijn *et al.*, 1990).

As shown in Figure 2.4, the change in the circular motion of the water particle is not the only property of the wave that is affected by a change in water depth. In shallow water, the wave crest travels faster than the rest of the wave resulting in the wave becoming vertically and horizontally asymmetric (Bosboom & Stive, 2012). While the changing wave properties in shallow water, such as the change in the vertical and horizontal asymmetry, cannot be described by the second-order Stokes theory. According to Van Rijn *et al.* (1990), the second-order Stokes theory is, however, most applicable in shallow waters, when H/h and H/L are small.

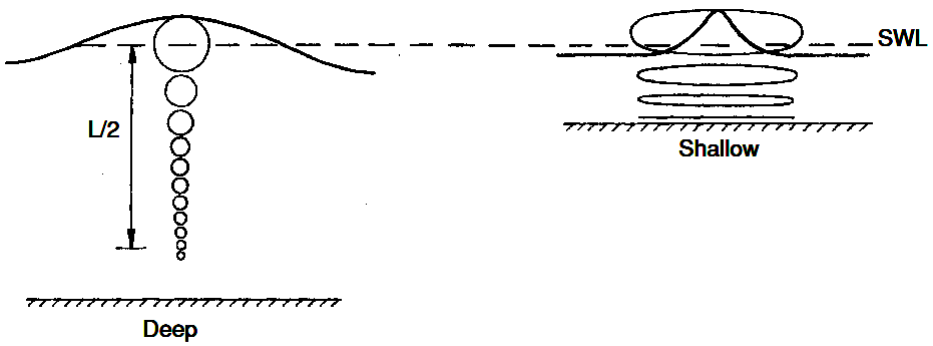

Figure 2.4. The change in the particle orbits as the water level changes (Sorensen, 2005).

In the process-based model formulated by Roelvink *et al.* (2009, 2010), the shallow water equations account for the non-linearity of waves in shallow water. The sediment transport formulas use the velocity calculated by the shallow water equations (Pender & Karunarathna, 2013).

2.2.3 Wave Profile Asymmetry and Skewness

The near-bed orbital velocities (U_{orb}) generated by the propagating waves reflect the changes in wave asymmetry and skewness (Boechat Albernaz *et al.*, 2019). The near-bed orbital

velocities are responsible for both onshore and offshore flow (Boechat Albernaz *et al*., 2019). The direction of near-bed orbital velocity below the crest of a wave is in the onshore direction while the orbital velocity below the trough is in the offshore direction. The deep water orbital velocity is commonly described using the fifth-order Stokes theory (Fenton, 1985), shown as

$$U_{orb} = \frac{\pi H_{rms}}{T_p sinh(2kh))} \tag{2.6}$$

where H_{rms} is the root mean square wave height, T_p is Wave period, k is wavenumber, and h is water depth. Waves become skewed during the shoaling processes, where the peaks increase and the troughs get flattened. Stokes' 2nd order theory best describes these processes (Bosboom & Stive, 2012), and Figure 2.1a shows a skewed wave. Asymmetric waves, otherwise known as second-harmonic waves, rapidly accelerate the water particles as the crest passes, and are mainly steep, Figure 2.1b. This rapid acceleration results in the mobilisation of the suspended sediment in the direction of motion (Boechat Albernaz *et al*., 2019). The wave is skewed when the wave becomes horizontally asymmetric. This is due to the trough of the wave becoming flattened and the crest peak, as shown in Figure 2.1a (Bosboom & Stive, 2012). Drake & Calantoni (2001) showed evidence of onshore sediment transport due to asymmetric waves in a field study carried out in Duck, North Carolina. As waves become skewed, this results in the direction of the net velocity in the offshore direction. The higher the wave asymmetry gets, the onshore to offshore flow is more gradual in comparison to the offshore to onshore flow (Fernández-Mora *et al*., 2015; Van Rijn, 2007). Therefore, more asymmetric waves contribute to the accretion of the near-shore zone. An example of this is as waves break, they become highly asymmetric and cause strong onshore acceleration which will encourage the onshore movement of sediment transport (Fernández-Mora *et al*., 2015). Figure 2.5 shows the horizontal asymmetry as the ratio of the horizontal distance, of the peak of the crest and this is described by $\Delta x_1/\Delta x_2$ for horizontal asymmetry and a_c/H for vertical asymmetry. However, the commonly used definitions are

$$As = \frac{\langle H(\eta)^3 \rangle}{\langle \eta^2 \rangle^{3/2}},\ Sk = \frac{\langle \eta^3 \rangle}{\langle \eta^2 \rangle^{3/2}} \tag{2.7}$$

where *As* is wave asymmetry, *Sk* is wave skewness, the brackets $\langle \cdot \rangle$ are time averages, *H* is the Hilbert transform, and η is water level.

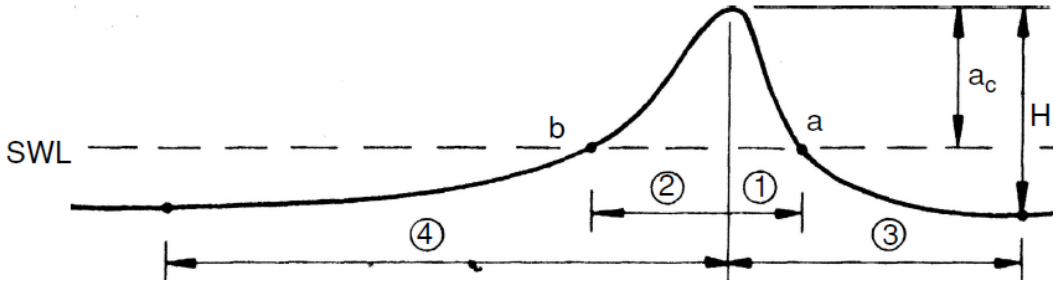

Figure 2.5. A simple distribution of the principles used to describe wave shape and compute asymmetry and skewness (Sorensen, 2005).

The sediment transport rate is a function of advection velocity and current flow velocity (Roelvink *et al.*, 2009, 2010). Advection velocity is a function of wave asymmetry, wave skewness and root mean squared velocity (U_{rms}) (Grasso *et al.*, 2011; Vousdoukas *et al.*, 2012), it is calculated as

$$U_a = (-w_1 As + w_2 Sk) U_{rms} \tag{2.8}$$

where U_a is the advection velocity, and w_1 and w_2 are the wave asymmetry and skewness calibrating factors applied to the wave skewness (*Sk*) and asymmetry (*As*) respectively (Roelvink *et al.*, 2009, 2010; Pender & Karunarathna, 2013). This is used in process-based models such as XBeach.

Van Thiel de Vries (2009) ran 72 simulations for varying values of wave asymmetry and skewness calibrating factors, and compared it to dune erosion wave flume data to select the optimal values for these calibrating factors. Van Thiel de Vries (2009) concluded that the optimal values for wave asymmetry calibrating factor and wave skewness calibrating factor that results in the smallest error is 0.1. The shortcoming of this optimization is that it was not done for an accretive case as well.

2.2.4 Radiation Stress

Radiation stress is a momentum flux of a fluid element, due to the wave-driven forces acting on the fluid element (Longuet-Higgins & Stewart, 1964). The cross-shore changes in radiation stress drive the generation of cross-shore currents, which are the main components of the cross-shore sediment transport (Dally & Dean, 1984).

The waves approaching the coast at an angle will result in three radiation stresses. The normal stress acting in the cross-shore and alongshore direction (x and y direction respectively), and the transport of x momentum in the y-direction (Bosboom & Stive, 2012). The first-order wave theory (Bosboom & Stive, 2012), describes radiation stresses as

$$S_{xx} = \left(n - \frac{1}{2} + \mathrm{n}\cos^2\theta \right) E \tag{2.9}$$

$$S_{yy} = \left(n - \frac{1}{2} + \mathrm{n}\sin^2\theta \right) E \tag{2.10}$$

$$S_{yx} = S_{xy} = \mathrm{n}\cos\theta\sin\theta\,\mathrm{E} \tag{2.11}$$

where E is the wave energy, n is the ratio of group velocity to phase velocity, C is the wave celerity, and θ is the wave approach angle. In the ideal situation for the study of cross-shore sediment transport where the waves approach the coastline perpendicular to the shoreline, there will only be normal stress acting in the x-direction and transport of x momentum in the y-direction. The cross-shore gradient of the change in the radiation stress is the main driving force of the cross-shore currents. The cross-shore currents result in the sediment transport in the cross-shore direction (Dally & Dean, 1984).

2.2.5 Bed Shear Stress

According to Montes (1998), the frictional force acting on the surface of the object that is in the path of the flowing fluid is called bed shear stress. However, if the object is in suspension

it will travel in the direction of the wave propagation. As waves propagate towards the shore, the changes in the horizontal and vertical asymmetry of propagating waves have a direct influence on the changes in the orbital velocities of the water particles and the magnitude of the bed shear stress experienced in the direction of the propagating wave. The direction of the bed shear stress is, therefore, continually changing directions with the direction of orbital velocity as a wave propagates (Wright *et al.*, 1999). Therefore, the direction of bed shear stress is in the direction of the net orbital velocities.

The orbital velocity of the particles is the speed of the particle that is in orbital motion due to the propagating waves (from crest to trough and back to the crest of the propagating wave), described in Equation 2.6. As the propagating wave gets into shallow waters, the wave height increases (shoaling) as the water depth decreases thus increasing the orbital velocity (Wright *et al.*, 1999; Bosboom & Stive, 2012). The shear stress is given by

$$\tau_c = \rho c_f |\vec{U}| \vec{U} \tag{2.12}$$

where c_f is a dimensionless coefficient, ρ density of the fluid, $\vec{U}$ is depth-averaged flow velocity in both the horizontal directions as well as in the cross-shore and alongshore direction. The bed shear stress is related to the depth-averaged current velocity and free stream velocity through the friction factor. The friction factor is a function of wave and current velocities. Bed shear is calculated in-terms of currents only in Equation 2.12 (Wright *et al.*, 1999; Ruessink *et al.*, 2001; Bosboom & Stive, 2012). Bed shear stress can be calculated with

$$\tau_{bx}^{E} = c_f \rho U_E \sqrt{(1.16 U_{rms})^2 + (U_E)^2} \tag{2.13}$$

where U_{rms} is the orbital velocity, U_E is the current flow velocity, c_f is $\sqrt{g/C^2}$, C is Chezy value of 55 $m^{1/2}/s$, and g is the gravity of Earth which is $9.81 m/s^2$. This is used in process-based models such as XBeach (Roelvink *et al.*, 2009, 2010).

2.2.6 Shallow Water Equation

The shallow water equation is a function of; the free surface and bottom boundary conditions, momentum equation, and continuity equation (Vreugdenhil, 2013). In XBeach, the shallow water equations calculate the Lagrangian velocity in both the cross-shore and alongshore direction (Andrews & McIntyre, 1978; Walstra *et al.*, 2001). However, in this study, only the cross-shore component is considered . The cross-shore component of the shallow water equation is

$$\frac{\partial U_L}{\partial t} + U_L \frac{\partial U_L}{\partial x} - v_h \left(\frac{\partial^2 U_L}{\partial x^2} \right) = \frac{\tau_{sx}}{\rho h} - \frac{\tau_{bx}^E}{\rho h} - g \frac{\partial \eta}{\partial x} + \frac{F_x}{\rho h} \tag{2.14}$$

where v_h is horizontal viscosity, τ_{bx}^E is the bed shear stress in the cross-shore direction, τ_{sx} is wind shear stress in the cross-shore direction, F_x is wave-induced stress, and η is the water level (Roelvink *et al.*, 2009, 2010).

The cross-shore component of the Lagrangian velocity is used to calculate current flow velocity (U_E) in the cross-shore direction. The advection and diffusion model uses the current flow velocity, in addition to the advection velocity, to calculate the depth-averaged sediment concentration in the water column. The current flow velocity is given by

$$U_E = U_L - U_S \tag{2.15}$$

$$U_S = \frac{E_w cos\theta}{hc} \tag{2.16}$$

where U_S is Stokes' drift in the cross-shore direction, E_w is wave-group varying short wave energy, θ represents the angle of wave approach, is density of the medium, h is the water depth, and c is wave speed.

2.3 Sediment Transport

Sediment transport is a function of both sediment properties, and the near-shore hydrodynamics and is the main driving factor of coastal profile change. In coastal areas, sediment transport takes place in both the alongshore and cross-shore direction depending on the approaching wave angle that the coastal area will experience. The rate of sediment transport shoreward of the breaker zone is mainly a function of local velocity (Kemp, 1975). The factors contributing to sediment transport are; the sediment properties, current-induced shear stress, and the slope of the beach (Hughes *et al.*, 1997). This study is based on the sediment characteristics found along the eastern coast of South Africa.

2.3.1 Sediment Properties

The sediment properties directly affect the sediment re-suspension, which in turn affects the sediment fall velocity. The sediment fall velocity is a function of the fluid's viscosity and density (Corey, 1949). Figure 2.6 shows the relationship between sediment properties, fluid characteristics and sediment transport. Dean & Dalrymple (2004), highlight the direct relationship between grain size, initiation of motion, and fall velocity. These properties have an effect on the sediment concentration in the water column and sediment deposition. The condition expressed by

$$\text{Instantaneous Fluid Force} > \text{Instantaneous Resting Force} \tag{2.17}$$

describes the conditions at which sediment particle initiation of motion will take place. The instantaneous resting force of the particle is a function of the particle weight and friction coefficient (Van Rijn, 2007).

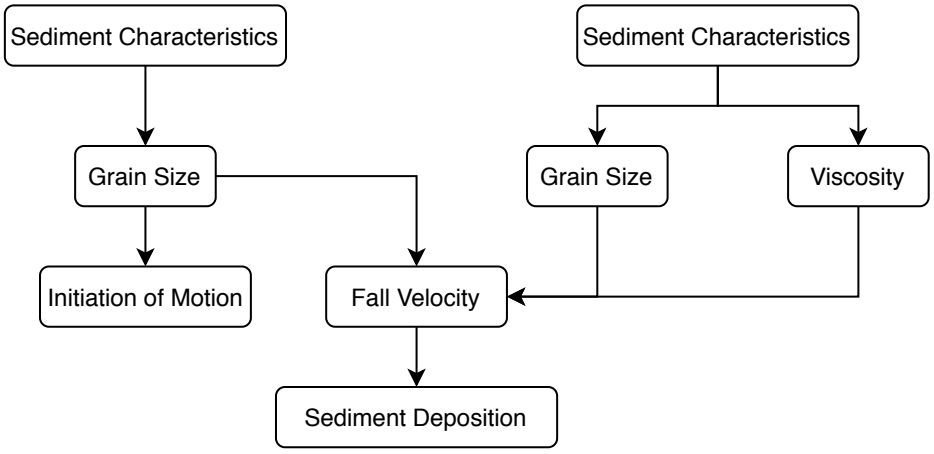

Figure 2.6. A description of how sediment and fluid characteristics contribute to sediment initiation of motion and deposition.

2.3.2 Cross-shore Transport and Coastal Sediment Sources

Cross-shore sediment transport is the function of sediment characteristics and wave actions. The coastal area is continually changing due to the net loss and gain of beach sand volumes both in the cross-shore and alongshore direction. Wave actions can either be destructive or constructive. The destructive forces contribute to the erosion of sand, and constructive forces contribute to accretion. An imbalance in the cross-shore radiation stress contributes to the generation of undertow, whereby a 2DV circulation current is generated in the breaker zone. In the breaker zone, the surface current is traveling towards the shore with an offshore flow occurring below the trough level (Bosboom & Stive, 2012; Lemos *et al.*, 2017). The main driving action of the cross-shore sediment transport is undertow. The undertow erodes the beach and deposits the sediments offshore. Undertow is, therefore, the main contributor to the formation of offshore sand bars. The steepness of the beach, in combination with gravity, plays a vital role in sediment transport in the cross-shore direction. A beach with a gradual slope will be able to distribute the wave energy over a greater cross-shore area than steeper beaches. Destructive forces are a result of high energy waves i.e storm events. Erosion takes place when the wave energy experienced by the coastal area is higher than that of its equilibrium energy. This usually happens during storm events in east coast of KZN with a significant wave height greater than 3.5 m (Corbella & Stretch, 2012b,c)

$$H_s > 3.5m \tag{2.18}$$

Accretive conditions are the result of low energy waves acting on the beach over a longer period relative to erosive conditions. Dean *et al*. (1973) proposed that erosion and accretion events could be assumed using the non-dimensionalized fall velocity, which is given by

$$\Omega = \frac{H_s}{wT_p} \tag{2.19}$$

where Ω is non-dimensionalized fall velocity, H_s is significant wave height, w is sediment fall velocity, and T_p is wave period (s). Conditions where $\Omega > 3,2$ will result in an erosive case and $\Omega < 3,2$ will result in an accretive case (Dean *et al*., 1973). Developing a sediment budget is essential to develop a good understanding of sediment movement in the coastal area. Sediment budget is otherwise known as the difference in the net change in volume of sand due to; erosion and accretion, sediment gains (sources), and losses (sinks) for a specific amount of time, which is described by

$$\sum Q_{Source} - \sum Q_{Sink} + \Delta V = Residual \tag{2.20}$$

where ΔV is change in volume within the cell due to erosion and/or accretion (m^3), $\sum Q_{Source}$ is sediment gains (m^3), $\sum Q_{Sink}$ is sediment loss (m^3). Developing a sediment budget for a coastal area assists in identifying the sediment sources, sediment transport direction as well as magnitude in both the cross-shore and alongshore direction, and sinks (Rosati, 2005). Sediment budget can also take into account dredging and pumping schemes, by refining Equation 2.20 as

$$\sum Q_{Source} - \sum Q_{Sink} - \Delta V + P - R = Residual \tag{2.21}$$

where P is the volume of material placed (m^3), and R is the amount of material removed from the beach (m^3). The perturbation of residual from 0 m^3 is a representation of the fluctuation of beach volume from the ideal equilibrium beach volume based on the sediment characteristics

of the beach. The time a beach takes to attain its pre-storm coastline shape and volume is called the recovery period (Corbella & Stretch, 2012c). This period is different for all the coastal areas throughout the world that are experiencing different wave conditions that are taking place at varying frequencies. The east of Kwazulu-Natal has a mean recovery rate of 97.3 $m^3m^{-1}yr^{-1}$ resulting in a recovery time of approximately 2 years (Corbella & Stretch, 2012c).

2.3.3 Equilibrium Beach Profile, Bar Formations and Transport

Net-Zero energy experienced by the near-shore environment means that a net-zero sediment transport. Hence, there will be no changes in the bed profile (Dean, 1991; Dean & Dalrymple, 2004). If the net energy experienced by a beach is zero, the beach profile will reach its equilibrium position (Dean, 1991; Dean & Dalrymple, 2004). Dean (1991) and Dean & Dalrymple (2004) highlighted that the equilibrium profile is a function of the sediment size and cross-shore distance, as given by

$$h = A(x^{2/3}) \tag{2.22}$$

where A is the sediment scale parameter, x is the cross-shore distance, and h is depth at a point in the cross-shore direction. The sediment scale parameter is a function of the sediment fall velocity, which in turn affects the slope of the profile calculated by Equation 2.22 (Dean, 1991; Dean & Dalrymple, 2004).

In the study conducted by Corbella & Stretch (2012c), using 37 years of beach profile data along the coastline of KZN indicates a periodic onshore and offshore volumetric sediment movement due to the periodic storm events and beach recovery period which was found to be an average of two years. Therefore, the ability of a model to reproduce accurate on-shore and off-shore sediment transport is crucial in providing an accurate description of the volumetric sediment flux in coastal areas. The formation of sandbars is the primary indication of cross-shore transport. The alongshore bars form due to the change in the

direction of net sediment transport found outside the surf zone (Deigaard *et al*., 1992). Figure 2.7 describes the formation of a bar. These bars travel onshore and offshore in response to the wave condition experienced by the beach. The offshore migration of a sandbar is due to the strong undertow generated by breaking waves over the bar (Thornton *et al*., 1996).

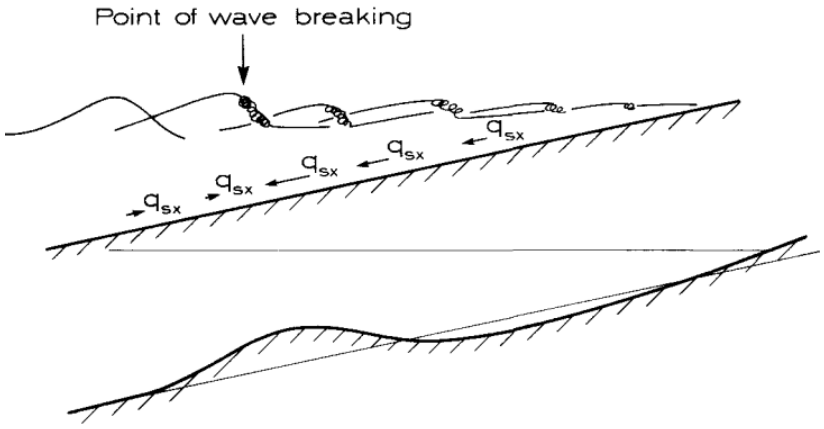

Figure 2.7. Differences in the direction of sediment transport within and outside the swash zone resulting in the formation of a sand bar (Deigaard *et al*., 1992).

Within the beach face, the inner surf and swash zone processes distribute the sand that has been eroded from the dune or brought onshore by the approaching waves (Van Thiel de Vries *et al*., 2007). The shallow water depth and the presence of turbulence complicate the hydrodynamics of the swash zone (Van Thiel de Vries *et al*., 2007). Therefore, while the beach profile can be closely related to the volume of sand on the beach. According to Jara *et al*. (2015) beach volume can also be closely related to the energy disequilibrium experienced. Kamphuis (2010) showed that the beach profiles are directly proportional to the wave energy of a series of waves approaching the beach face.

2.4 Process-Based Models

Process-based models such as Delft3D and XBeach are designed to simulate and analyse coastal processes, and extreme wave conditions (Roelvink, 2003; Roelvink *et al*., 2009, 2010). Delft3D simulates spectral waves, hydrodynamics as well as the resulting sediment transport. Previous research indicates that the sediment transport models in Delft3D are

capable of accurately simulating specific cross-shore erosion and accretion events through calibration. Wells (2015) researched the capacity of the sediment transport models available in Delft3D to simulate realistic sediment transport during erosion and accretion events. The parameters, shown in Table 2.2, are varied to simulate realistic sediment transport during erosion and accretion events.

Table 2.2 Parameters used to calibrate the sediment transport models in Delft3D.

Sediment Transport Model	**Calibrating Parameter**	
Van Rijn Model	fsus	user-defined tuning parameter
Bijker-Bailard Model	Afac	user-defined calibration coefficient for the wave asymmetry
Soulsby-van Rijn Model	None	

Wells (2015) showed that Delft3D sediment transport models could not simulate realistic cross-shore erosive and accretive events without varying the calibrating parameters separately for erosive and accretive events. Pender & Karunarathna (2013) modelled beach profile variability using a statistical approach and XBeach. XBeach can accurately simulate beach erosion events without calibration of the asymmetry and the skewness calibrating factors. However, a higher wave asymmetry calibrating factor, which in turn results in higher onshore sediment transport, results in accretion events (Pender & Karunarathna, 2013). Therefore, the relationship between the wave asymmetry calibrating factor and the resulting sediment transport must be quantified. Furthermore, the validation of the relationship quantified using real-world data will enable the selection of appropriate values for the calibrating factors that results in a realistic sediment transport for the given wave conditions. This study explores; the relationship between the sediment transport rates and varying wave asymmetry and wave skewness calibrating factors as well as the approaching wave energy.

2.5 XBeach Model

XBeach is a near-shore numerical model that is used to simulate the response of the coastal area to time-varying storm and hurricane conditions (Roelvink *et al.*, 2009, 2010). The wave

models in XBeach include wave transformation. XBeach uses a roller and wave dissipation model to cater for the variation in wave energy per wave group. Furthermore, depth-averaged shallow water equations, and advection and diffusion equations are used to account for time-varying wave forcing terms and solve for the depth-averaged sediment concentration, respectively. The morphological changes are as the result of hydrodynamic processes coupled with the sediment transport models available, as discussed in section 2.5.2. A description of the different components that XBeach consists of is displayed below in Figure 2.8. XBeach is mainly developed and validated to simulate dune erosion due to energetic wave conditions (Bolle *et al*., 2011). The hydrodynamics processes consist of three-wave models, and the sediment transport module consists of three formulae as discussed in Section 2.5.2.

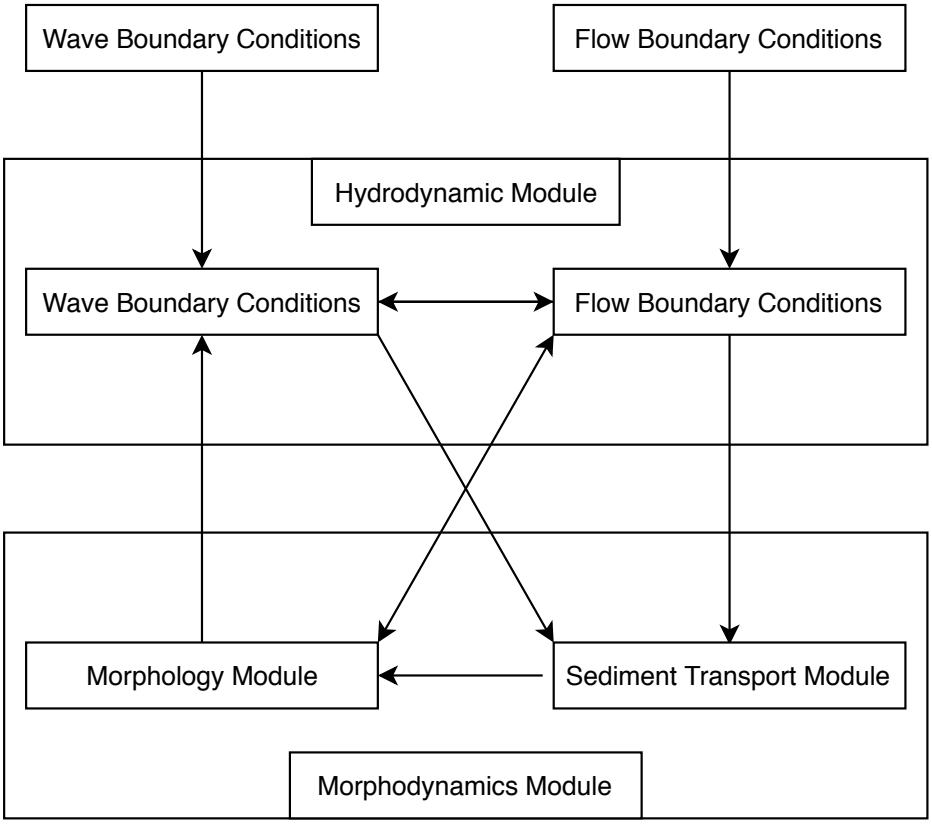

Figure 2.8. The component modules that are available in XBeach. The arrows indicate connectivity.

2.5.1 Morphodynamic Processes

The majority of coastal areas around the world consist of a variety of materials ranging from fine sand to large pebbles (i.e., shingles). The dynamic conditions experienced by the coastal areas result in the constant evolution of their profiles and shoreline positions both in the cross-shore and alongshore directions. The constant changes of the beach profiles are due to sediment transport in the near-shore environment, in response to perturbation of the wave energy experienced by the coastal area from the equilibrium wave energy, of the respective beach. The current and wave-induced velocities are the main contributors to sediment transport within coastal environments. The morphological changes are modelled as shown in Figure 2.9. In this study, the three sediment transport models used are the Van Rijn (Van Rijn *et al.*, 1993), the Van Thiel-Van Rijn (Van Rijn, 2007) and the Soulsby-van Rijn model (Soulsby, 1997a). These sediment transport models are coupled with the wave model to compute the morphological changes occurring due to sediment transport. Changes in the morphology of the coastal areas have a direct impact on the near-shore hydrodynamics such as changes in the current flow velocity and orbital velocity, U_{rms}, which in turn affects the sediment transport in response to the newly calculated hydrodynamics.

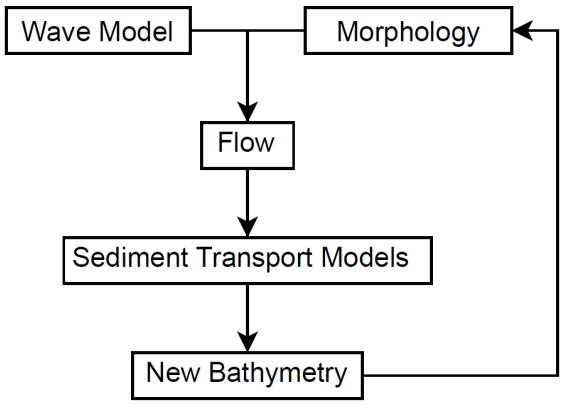

Figure 2.9. XBeach morphodynamic processes.

The sediment transport models are used to compute the equilibrium sediment concentration, that is used as a source term in the advection-diffusion model, as discussed in section

2.5.2, to calculate the depth-averaged sediment concentration. The depth-averaged sediment concentration is thereafter used to compute the sediment transport rate as a function of cross-shore position and time, which is given as

$$q_t = C_s U_{reps} - D_h h \frac{\partial c}{\partial x} - 1.6 C_s V_{magu} \frac{\partial z}{\partial x} \tag{2.23}$$

where C_s is the depth-averaged sediment concentration, U_{reps} is $E + U_a$, D_h is the sediment diffusion coefficient, and V_{magu} is the Lagrangian transport velocity. The bed level change as a function of time is directly related to the sediment transport gradients in the cross-shore direction. A morphological change scaling factor is available in the bed level change computation. However, cross-shore sediment transport is more instantaneous in comparison to alongshore transport. Avalanching is taken into account for both wet and dry sand. Once the critical slope has been reached, avalanching will take place.

2.5.2 Process-Based Sediment Transport Models

Computing the movement of sediment as a function of the wave conditions, and sediment characteristics are essential for the prediction of the coastal morphology, and development of a deeper understanding of sediment dynamics in a coastal system. There are a variety of semi-empirical sediment transport models that have been validated using multiple flume tests. In this review, the sediment transport formulas discussed are limited to those used by XBeach. XBeach uses a depth-averaged advection-diffusion equation proposed by Galappatti & Vreugdenhil (1985) to compute the flux of suspended sediment in slow varying flows, given by

$$\frac{\partial h C_s}{\partial t} + \frac{\partial h C_s (U_E - U_a cos\theta_m)}{\partial x} + \frac{\partial}{\partial x}\left[D_h h \frac{\partial C_s}{\partial x}\right] = \frac{h C_{eq} - h C_s}{T_s} \tag{2.24}$$

where C_s is the depth averaged sediment concentration, U_E is the current flow velocity, U_a is the advection velocity, D_h is sediment diffusion coefficient, C_{eq} is the equilibrium sediment concentration, θ_m is wave approach direction, and T_s is adaptation time. The sediment concentration is computed using equation 2.24 (Galappatti & Vreugdenhil, 1985). The

wave conditions such as approach direction (θ_m), wave asymmetry, and wave skewness have an effect on the rate and direction of transport. The sediment transport rate is estimated as a function of the current flow velocity, and advection velocity, as shown in Equation 2.23. XBeach has three process-based transport models used in the computation of sediment transport formulas that are used to compute C_{eq}. The models are; the Van Rijn (Van Rijn *et al.*, 1993), the Van Thiel-Van Rijn (Van Rijn, 2007) and the Soulsby-van Rijn model (Soulsby, 1997a). Although in XBeach, there are no user-defined calibration parameters within the formulas, there are however calibration parameters capable of optimising the sediment transport; such as the wave asymmetry (w_1) and wave skewness calibrating coefficient (w_2).

Van Rijn (1993) Model

Initially the Van Rijn model (Van Rijn, 1984) was used without the effect of waves. However, the latest adaptations (Van Rijn *et al.*, 1993) take into consideration the effect of waves. This sediment transport formulation calculates the bed transport as a function of the; sediment mobility number, sediment characteristics, and excess sediment mobility number i.e., it is estimated using the critical velocity . The bed transport formulation is

$$Sb = 0.006\rho_s w_s D_{50} M^{0.5} M_e^{0.7} \tag{2.25}$$

where M is sediment mobility number due to waves and currents ($\frac{v_e^2}{(s-1)gD_{50}}$), D_{50} is the sediment diameter, M_e is excess sediment mobility number ($v_e - v_{cr}$), w_s is sediment fall velocity, and D_{50} is the sediment diameter. The sediment transport above the reference height is considered to be suspended sediment transport (Van Rijn *et al.*, 1993). The advection-diffusion equation is used to solve for the depth-averaged sediment concentration calculated, which is thereafter used to calculate the sediment transport rate. The sediment concentration is calculated as

$$c_a = 0.015\rho_s \frac{D_{50} T_a}{\alpha D_*^{0.3}} \tag{2.26}$$

where ρ_s the density of the sand, D_{50} is the sediment diameter, D_* is the dimensionless sediment diameter, T_a is the bed shear stress parameter, and α is the reference level.

Soulsby-Van Rijn and Van Thiel-Van Rijn Model

The Soulsby-Van Rijn formula is derived from the application of Grass (1981) to the Van-Rijn, current alone, formula. Additionally, the formula is modified to consider both threshold and a slope term (Soulsby, 1997a,b). The critical velocities are calculated in a depth averaged sense. Furthermore, the drag coefficient is used as it takes into account the drag/resistance of a sand particle in a fluid environment.

The equilibrium sediment concentration (C_{eq}) is computed separately for bed ($C_{eq,b}$) and suspended ($C_{eq,s}$) loads as

$$C_{eq,b} = \frac{A_{sb}}{h}\left(\sqrt{V_{mg}^2 + 0.018\frac{U_{rms}^2}{C_d}} - U_{cr}\right)^{2.4} \tag{2.27}$$

$$C_{eq,s} = \frac{A_{ss}}{h}\left(\sqrt{V_{mg}^2 + 0.018\frac{U_{rms}^2}{C_d}} - U_{cr}\right)^{2.4} \tag{2.28}$$

where D_{50} is the sediment diameter, U_{cr} is the threshold current velocity , D_* is the dimensionless sediment diameter, V_{mg} is the velocity magnitude ($\sqrt{U_L^2 + U_S^2}$), C_d is the drag coefficient due to current alone, and A_{sb} and A_{ss} are the bedload and suspended load coefficients given as

$$A_{sb} = 0.005h(\frac{D_{50}}{h\Delta g D_{50}})^{1.2}, \quad A_{ss} = 0.012 D_{50}\frac{D_*^{-0.6}}{(\Delta g D_{50})^{1.2}} \tag{2.29}$$

In the Soulsby-van Rijn model, the equilibrium sediment concentration is a function of the bedload and suspended load coefficients (A_{sb} and A_{ss}, equation 2.29), the orbital velocity with turbulence approximation to account for the wave breaking induced turbulence, in response to; short waves (U_{rms}), critical velocity (U_{cr}), and depth-averaged current velocity (V_{mg}).

The Van Thiel-Van Rijn, sediment transport formulation, is similar to the Soulsby-Van Rijn sediment transport formulation with two major differences. Firstly, the drag coefficient is not calculated and incorporated into the equilibrium sediment concentration computation, and secondly the critical velocity is calculated separately for currents and waves, and when summed with a calibrating factor, is applied to compute critical velocity given by

$$U_{cr} = \beta U_{crc} + (1-\beta)U_{crw} \tag{2.30}$$

where β is

$$\beta = \frac{V_{mag}}{V_{mag} + U_{urms}} \tag{2.31}$$

This is used to estimate the equilibrium sediment concentration presented as

$$C_{eq,b} = \frac{A_{sb}}{h}\left(\sqrt{v_{mg}^2 + 0.64U_{rms}^2} - U_{cr}\right)^{1.5} \tag{2.32}$$

$$C_{eq,s} = \frac{A_{ss}}{h}\left(\sqrt{V_{mg}^2 + 0.64U_{rms}^2} - U_{cr}\right)^{2.4} \tag{2.33}$$

where D_{50} is the sediment diameter, U_{cr} is the threshold current velocity , D_* is the dimensionless sediment diameter, V_{mg} is the velocity magnitude ($\sqrt{U_L^2 + U_S^2}$), C_d is the drag coefficient due to current alone, and A_{sb} and A_{ss} are the bedload and suspended load coefficients given as

$$A_{sb} = 0.0015h\frac{(D_{50}/h)^{1.2}}{(\Delta g D_{50})^{0.75}}, \quad A_{ss} = 0.012D_{50}\frac{D_*^{-0.6}}{(\Delta g D_{50})^{1.2}} \tag{2.34}$$

Pender & Karunarathna (2013) uses the Van Thiel-Van Rijn formulae to simulate beach recovery while the Soulsby-van Rijn formulae were used to simulate erosion due to storm events with an average Brier Skill Score (BSS) of 0.755 for both cases and formulations.

CHAPTER 3: MATERIALS AND METHODS

This chapter presents the procedures followed in the model setup, which consists of the selection of the beach slope, model grid, sediment characteristics, time frame, wave conditions, and flow boundary conditions. Furthermore, the simulation structure followed is described in this chapter.

3.1 XBeach Cross-Shore Model Setup

XBeach is used in the development of early warning systems, research of beach recovery, as well as the study and modelling of shoreline evolution (Vousdoukas *et al*., 2012; Pender & Karunarathna, 2013). To produce realistic results from models such as XBeach, the ever-changing bed profile, and the related near-shore hydrodynamics must be accurately resolved. Therefore, the ability of XBeach to produce realistic bed profile and shoreline position changes is essential.

3.1.1 Cross-Shore Profiles and Model Grid

The cross-shore profile used in this study has a slope of 0.02, as shown in Figure 3.1. The beach cross-shore profile properties are:

- D_{50} of 0.355 mm,
- Profile width of 690 m, and
- Depth at the offshore boundary of 10 m.

Figure 3.2 shows the variations of horizontal spacing in the cross-shore direction as a function of the water depth. This was performed to ensure that the physical processes can be better resolved. The number of grid cells in the vertical is the same throughout the cross-shore

domain. However, the spacing of the vertical layer is a function of the water depth. Therefore, to ensure the stability of the model in the swash zone and thereby keep the time step from becoming too low, where the waters are shallow, the horizontal spacing is decreased with the decreasing water depth. The time step is calculated using

$$\Delta t = \frac{CFL\Delta x}{u} \tag{3.1}$$

where CFL is Courant-Friederichs-Lewy number (Roelvink *et al.*, 2010; Vousdoukas *et al.*, 2012) , u is the magnitude of the velocity in the horizontal direction, Δt is time step, and Δx is the horizontal grid spacing.

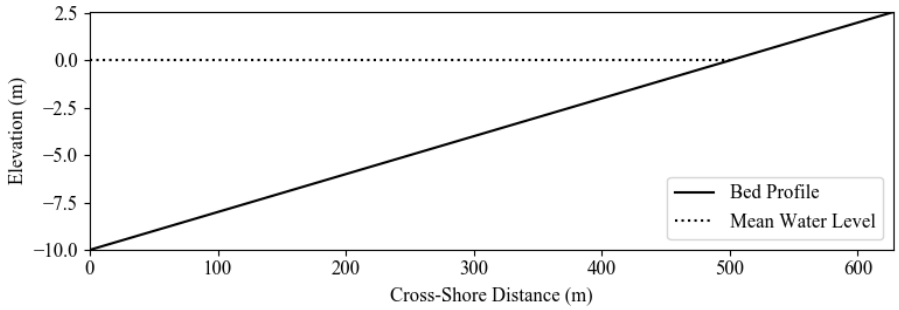

Figure 3.1. The beach profile used in this study. This profile has a slope of 0.02 and D_{50} of 0.355 mm. The dotted line indicates the mean water level, and the solid line indicates the bed profile.

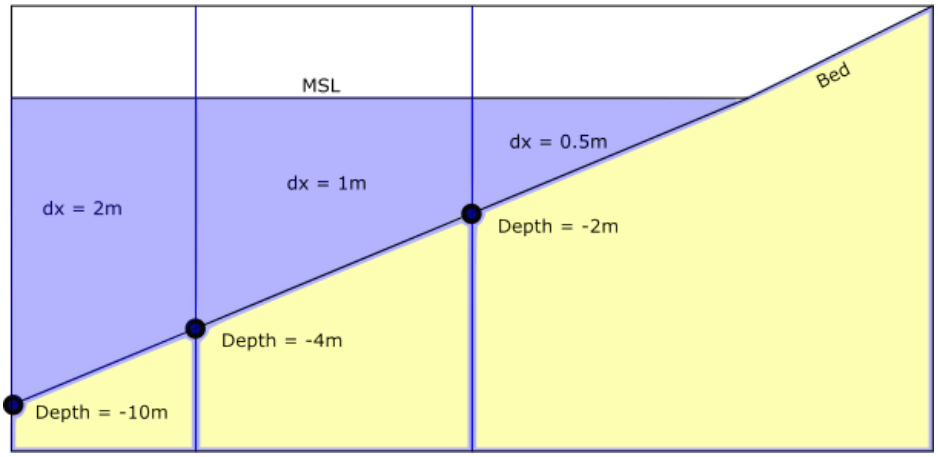

Figure 3.2. The horizontal grid spacing change in the cross shore domain, where dx is horizontal grid spacing.

3.1.2 Flow Boundary Conditions

The waves approach the shore perpendicular to the beach face. This is achieved by setting the mean wave direction, and the orientation of the beach, as described in Table 3.1. Figure 3.3 explains the boundary setup parameters. The offshore and onshore boundary of the model are setup as the absorbing-generating (weakly-reflective) boundary in 1D. Active reflection compensation (hereafter ARC) at the seaward boundary, is enabled to prevent the re-reflection of outgoing waves within the model. The mean wave propagation direction used is a representative of the unidirectional propagation of short wave fronts. Hence, no directional spreading took place.

Table 3.1 Key parameters used to describe the beach orientation.

Parameter	**Unit**	**Value**
Orientation of the beach [mainang]	[deg]	0
Wave direction [alfa]	[deg]	270

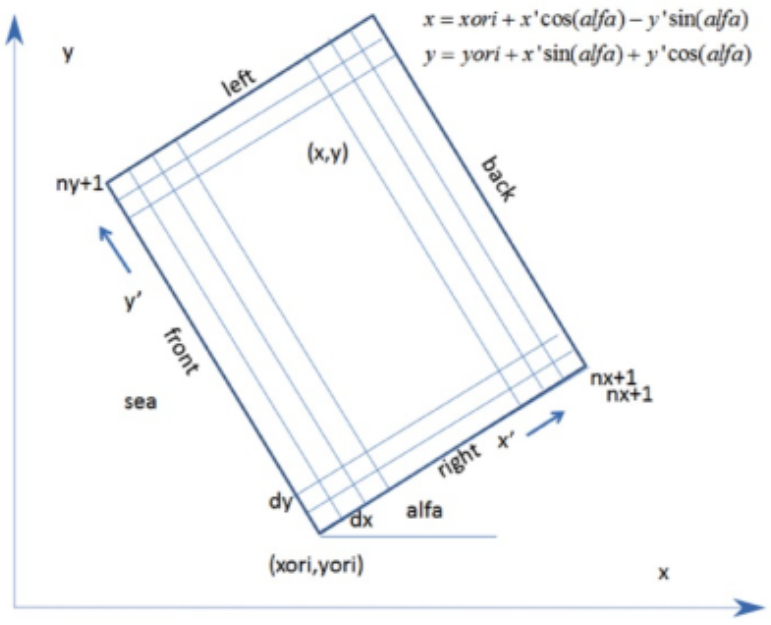

Figure 3.3. The Rectangular co-ordinate system of XBeach

3.1.3 Sediment Characteristics

The sand-size selected is the representative of the KZN coastline. Sediment characteristics data collected by EMS (2007-2011) for the coastal area that lies between the Mgeni River and Umhlanga. The coastal area stretching from the Mgeni River to Umhlanga is made up of sand-size (D_{50}) ranging from 0.125 mm to 4.0 mm, as shown in Figure 3.4. Figure 3.5 shows the first, second, and third quantile (Q_1, Q_2, and Q_3, respectively), and 95^{th} percentile of the percentage of sediment retained in each sieve class size for eight samples taken and analyzed over three years ranging from 2009 to 2011, presented in Appendix B.

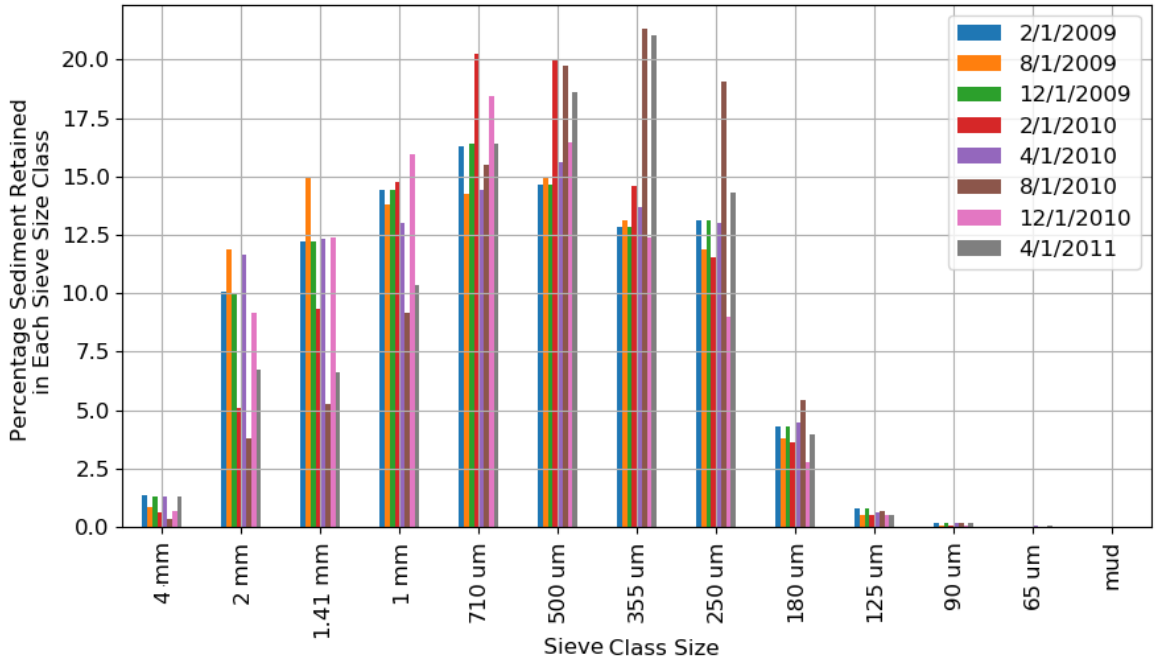

Figure 3.4. The percentage of sediment retained in each sieve class size for samples from Mgeni River to Umhlanga (2009-2011). The coastal area where the samples were obtained from is displayed in Appendix B.

The 95^{th} percentile of the average percentage of sediment retained in each sieve size for samples taken from the coastline on eight different dates between 2009 and 2011 indicates that the majority of the coast consists of sand with a D50 of 0.355 mm, as shown in Figure 3.5. Based on this analysis, a sediment size of 0.355 mm is selected to simulate the sand on the beach slope in this study as it is the representative of the KZN coastline.

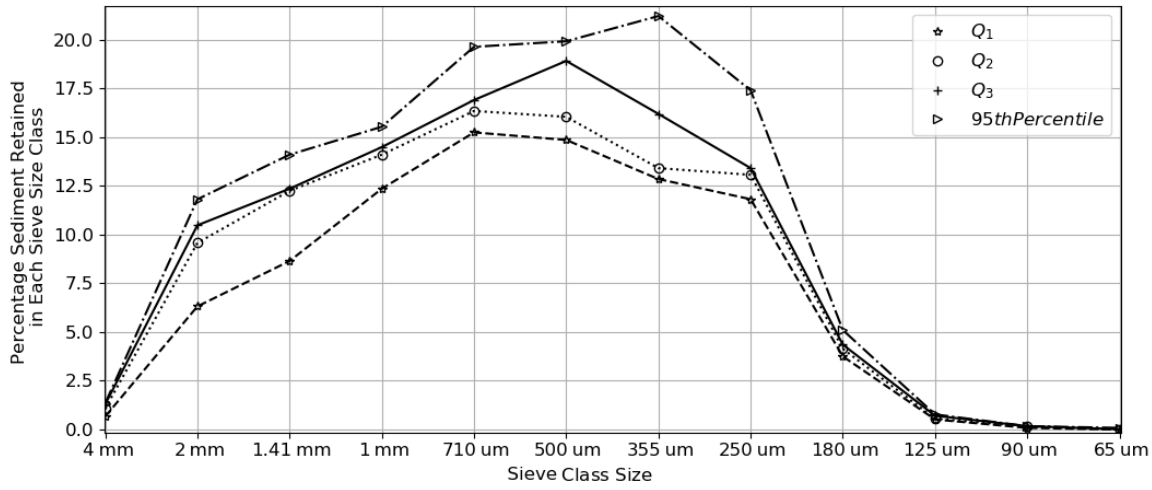

Figure 3.5. The first, second, third quantile (Q_1, Q_2, and Q_3, respectively) and 95^{th} percentile showing the average percentage of sediment retained in each sieve class size for samples taken from the coastline, stretching from the Mgeni River to Umhlanga in the KZN coastline.

3.1.4 Time Frame

All simulations were run in surfbeat mode for a period of 1.5 simulation days (simulation days are the number of days that the event is simulated for) for the high energy wave condition, and 1.5 simulation days for the low energy wave condition. A morphological acceleration of 10 was used for the low energy wave condition simulations, which simulated morphological changes for 15 simulation days. The beach slope was exposed to the varying wave conditions, shown in Table 3.2, which resulted in an accretive and erosive state. The rate and direction of the resulting sediment transport is investigated. Hence, the time frame chosen was sufficient to allow a clear picture of cross-shore transport to develop .

3.1.5 Wave Boundaries Conditions

The wave height and period was chosen from nine years of wave data obtained from the wave rider buoy offshore of the Durban harbour. The wave heights and corresponding wave periods are displayed in Figure 3.6. The non-dimensionalized fall velocity is given as

$$\Omega = \frac{H_s}{wT_p} \tag{3.2}$$

where Ω is non-dimensionalized fall velocity, Hs is significant wave height (m), w is sediment fall velocity (m/s), and Tp is wave period (s), was used to estimate wave conditions for the desired outcome.

Figure 3.6 shows that the erosive waves have periods greater than 7.5 s. However, the majority of wave heights that are greater than 3.5 m have periods that fall in a range of 10 to 12 s. Hence, a high energy wave condition with a period of 11 s was selected while a low energy wave condition with the same period was selected for consistency. The relationship between wave height (H_s) and the dimensionless fall velocity (Ω) is linear.

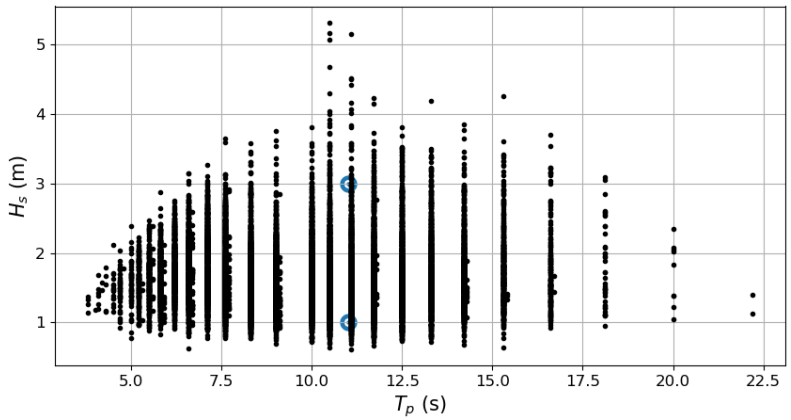

Figure 3.6. Wave characteristics observed from 2007-2016. Where the blue dots indicate the selected wave conditions.

The two wave conditions used are chosen using the dimensionless sediment fall velocity to result in accretive and erosive conditions. Higher wave heights results in a higher non-dimensional fall velocity, as discussed in section 2.3.2. In the KwaZulu-Natal coastal area, waves can be classified as a storm waves if they are greater than 3.5 m (Corbella & Stretch, 2012b).

Table 3.2 Summary of the wave conditions tested. The power spectrum density (PSD) of the wave input is shown in Figure 3.7.

Condition	H_s **(m)**	**Tp (s)**	**ws** ($\frac{m^2}{s}$)	**Ω(-)**	**Expectation**
1	1	11	0.034	1.753842	Accretion
2	3	11	0.034	5.261527	Erosion

The imposed wave condition is approaching the beach perpendicularly, so wave refraction is not taken into consideration. Furthermore, the model is 1D with vertical layers. This means that there was no need to consider the alongshore components of the linear, and shallow water equations.

3.1.6 Wave Model

Corbella and Stretch (2014) stated that a JONSWAP spectrum could best describe the wave conditions along the east coast of KwaZulu-Natal. A JONSWAP spectrum, with the largest recommended peak enhancement factor of five, was used to simulate the wave spectrum. Table 3.3 shows the parameters utilized to describe the JONSWAP spectrum, that was used to simulate the varying wave conditions explored in this project.

Table 3.3 Summary of the JONSWAP spectrum used.

Parameter	**Unit**	**Value**
H_s of the wave spectrum, significant wave height	[-]	1m and 3m
Peak enhancement factor in the JONSWAP expression	[-]	5
Directional spreading coefficient	[-]	1
Main wave angle (nautical convention)	[deg]	270
Peak period of the wave spectrum	[s]	11

XBeach has five different wave breaking formulations used for short wave dissipation. The wave breaking model used in this project was formulated by Roelvink (1993). This wave breaking formulation has a breaker index where wave breaking starts when the H/h ratio is higher than the set breaker index threshold. The selected wave breaking model allows for the specification of the breaker index. The breaker index of 0.78 was used because the propagating wave only makes contact with the bed as the wave-height to water-depth ratio reaches 0.77 (Roelvink, 2011). The JONSWAP spectrum of the wave conditions selected is described in Figure 3.7. The characteristics of the selected spectrum are displayed in Table 3.3.

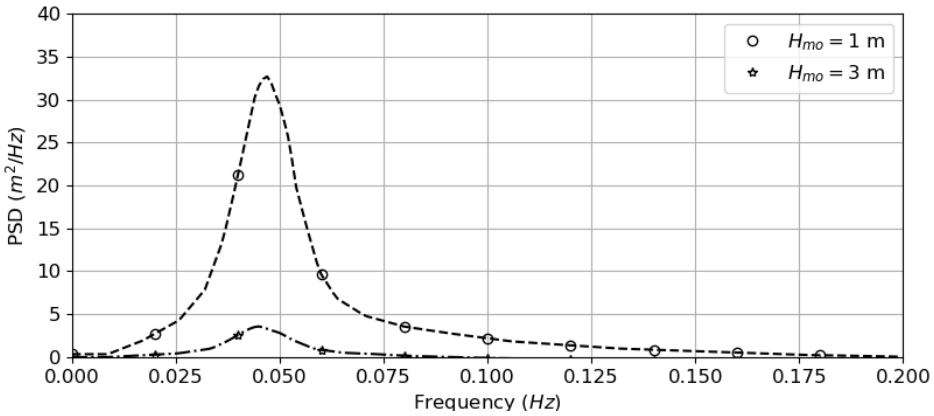

Figure 3.7. Power Spectrum Density (PSD) of wave condition 1, and wave condition 2.

XBeach uses an explicit numerical solution scheme, where the user specifies the Courant-Friedrichs-Lewy number (CFL), and the model computes an automatic time-step each time, thus guaranteeing stability. In this study, a CFL value of 0.7 was used.

3.2 Simulation Structure

The parameters used to calibrate the model in this study were the wave asymmetry and wave skewness. The surfbeat and stationary mode in XBeach allow the calibration of w_1 (wave asymmetry calibrating factor), and w_2 (wave skewness calibrating factor). These parameters are only functional in the surfbeat and stationary wave model (wave averaged). The non-

hydrostatic model is a wave resolving model. Therefore the pre-described parameters cannot be used as the wave asymmetry and wave skewness is explicitly resolved. The sediment transport formulas used in XBeach do not have parameters that can be varied individually to change the sediment transport rate. Therefore, the w_1 and w_2 parameters adjust the wave asymmetry and wave skewness contributions, which in turn affects the net sediment transport rate and direction. The chosen parameter is varied from 0 to 1 for wave conditions discussed in Section 3.1.5. The simulation was made to write-out at a time interval of 1s for the instantaneous output variables and every 1800s for the mean, max, and min output variables.

The input for the simulation includes the sediment characteristics (i.e., sediment size), simplified morphological characteristics (i.e., beach slope), and idealized wave climate (i.e., wave height, wave period). Figure 3.8 shows the schematic diagram of the simulated experimental data. Due to limitations in the amount of long-term data available for wave climate, beach morphology (slope), and sediment characteristics for a given beach, XBeach was used to simulate and explore the relationship between these variables. The simulations were set up to consider all the aforementioned characteristics. The wave asymmetry and thereafter, the wave skewness calibrating factors, were varied independently to analyse the sensitivity of the advection velocity, sediment transport rate, as well as sediment transport direction. Initially, the wave asymmetry calibrating factor was increased from 0-1. Once completed, the wave skewness calibrating factor was increased from 0-1. Thereafter, the wave asymmetry and wave skewness calibrating factors were increased simultaneously from 0-1, and increased at an interval of 0.1. The detailed model setup can be found in Appendix A. The wave asymmetry and wave skewness calibrating factors were used in the calculation of the sediment transport rate through the advection velocity, that is calculated as

$$U_a = (w_1 \ Sk - w_2 \ As) \ U_{rms} \tag{3.3}$$

where w_1 and w_2 are the wave asymmetry and wave skewness calibrating factors applied to the wave skewness (Sk) and asymmetry (As) respectively. The advection velocity was

then used to calculate the representative velocity, that was used in the sediment transport rate calculations with

$$q_t = C_s U_{reps} - D_h h \frac{\partial c}{\partial x} - 1.6 C_s V_{magu} \frac{\partial z}{\partial x} \tag{3.4}$$

where C_s is the depth-averaged sediment concentration, U_{reps} is $U_E + U_a$, D_h is the sediment diffusion coefficient, V_{magu} is the Lagrangian transport velocity, U_a is the advection velocity, and U_E is current flow velocity.

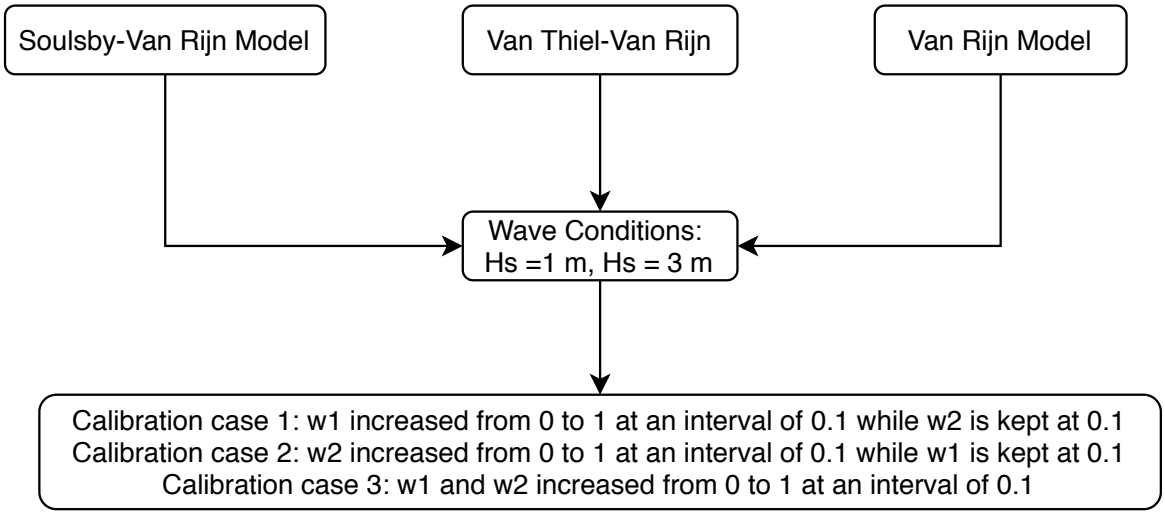

Figure 3.8. The schematic diagram of the experimental design of the simulation run per wave condition selected.

CHAPTER 4: RESULTS AND DISCUSSION

This chapter presents the results and discussion on the effect of varying wave asymmetry (w_1) and wave skewness (w_2) calibrating factors on the hydrodynamics and the sediment transport models available in XBeach (i.e Soulsby-Van Rijn model, Van Thiel-Van Rijn model, and Van Rijn model), as well as the capacity of the available sediment transport models to simulate beach erosion and accretion under fixed model parameters with varying wave conditions. The wave conditions that will result in accretion and erosion are estimated using Dean's Heuristic model, otherwise known as the non-dimensionalized fall velocity (Ω).

4.1 Hydrodynamics

There is a direct relationship between the current flow velocity (U_E) and the sediment transport direction. Negative (offshore) current flow velocities will result in an offshore sediment transport and positive (onshore) current flow velocities will result in onshore sediment transport. The time-averaged current flow velocity for both wave conditions investigated was found to be in the offshore direction. Figure 4.1 displays the first decile, first quantile, second quantile, third quantile, and ninth decile of the current flow velocities. This statistical analysis of the current flow velocities for the wave spectrum ran, with H_s of 1 m and 3 m shows that the beach experiences a negative (offshore) velocity majority of the time. That is indicated by the second quantile (median) being negative. The advection velocity (U_a) was found to increase linearly (for both wave conditions) with the increasing wave asymmetry calibrating factor (w_1) relative to wave skewness calibrating factor (w_2) and increasing wave skewness calibrating factor (w_2) relative to wave asymmetry calibrating factor (w_1), as shown in Figure 4.3.

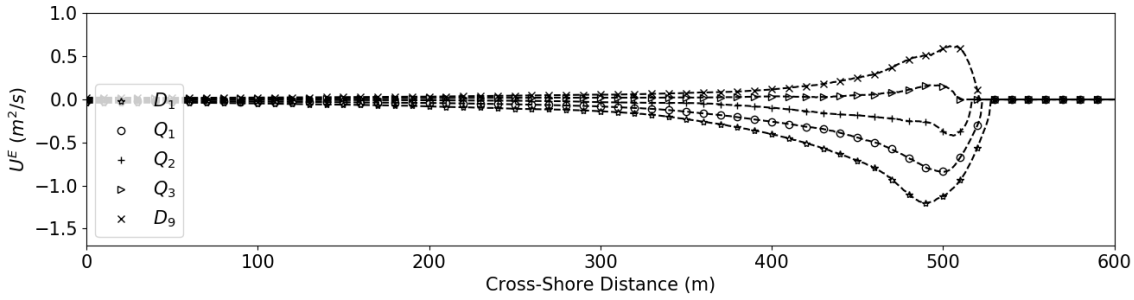

Figure 4.1. The first decile (D_1), first quantile (Q_1), second quantile (Q_2), third quantile (Q_3), and ninth decile (D_9) of the current flow velocities due to a wave height of 1 m.

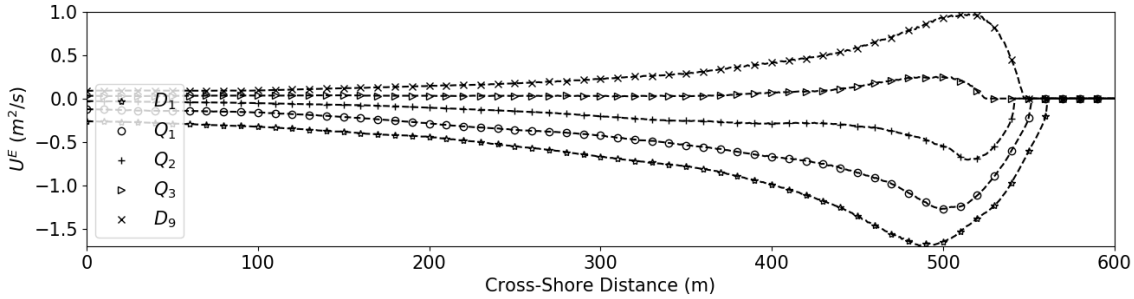

Figure 4.2. The first decile (D_1), first quantile (Q_1), second quantile (Q_2), third quantile (Q_3), and ninth decile (D_9) of the current flow velocities due to a wave height of 3 m.

Non-dimensionalizing the advection velocity in terms of the wave height and wave period allows for the exploration of a wide variety of wave conditions i.e. wave height and period (Non-dimensionalizing of the advection velocity is presented in Apendex A). Furthermore, the Non-dimensionalizing helps to estimate the expected magnitude and direction of the advection velocity as a function of the wave asymmetry calibrating factors or wave skewness calibrating factors (w_1 and w_2, respectively). The representative velocity (Urep) is the sum of the advection velocity and current flow velocity, given by

$$U_a = (-w_1 As + w_2 Sk) U_{rms} \tag{4.1}$$

where w_1 and w_2 are the wave asymmetry and wave skewness calibrating factors applied to the wave skewness (Sk) and asymmetry (As) respectively.

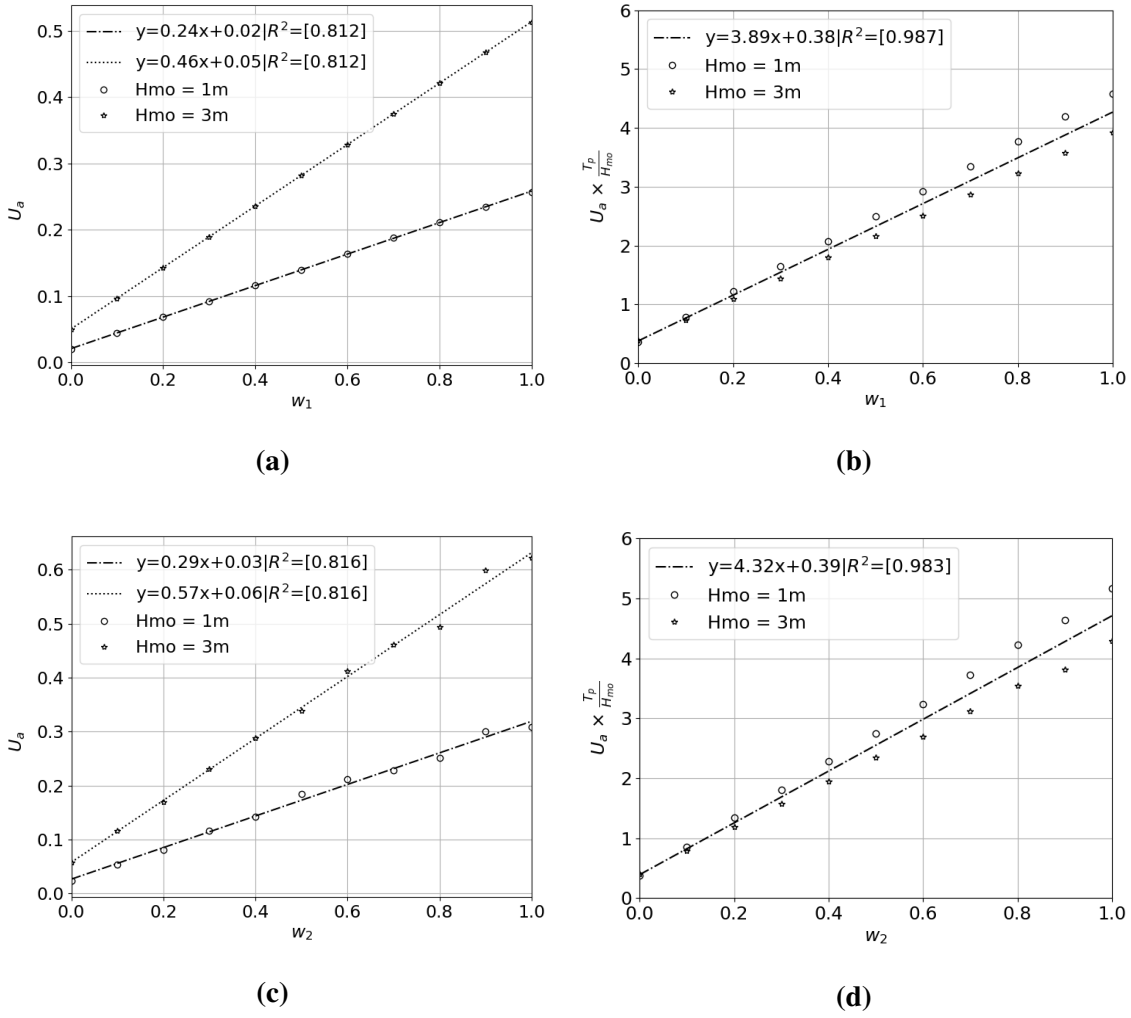

Figure 4.3. The change in the advection velocity as a function of the wave asymmetry (w_1) and wave skewness calibrating factors(w_1) displayed in (a) and (c), respectively. The dotted and dashed lines are the best-fit lines for H_s of 1 m and 3 m. The change in non-dimensionalizing advection velocity as a function of the wave asymmetry calibrating factors (w_1) and skewness calibrating factors (w_2) is displayed in (b) and (d), respectively.

Given the above mentioned results, the change in the wave asymmetry calibrating factor (w_1) relative to wave skewness calibrating factor (w_2) and wave skewness calibrating factor (w_2) relative to wave asymmetry calibrating factor (w_1) will have a direct effect on the sediment transport rate as well as direction. This is due to the incorporation of short wave non-linearities in the computation of the advection velocity (U_a), which is used in addition to the current flow velocity (U_E) to calculate the sediment transport rate, as shown in Equation 4.2. The offshore flow of the time-averaged current flow velocity, in addition to the offshore

direction of the advection velocity under default w_1 and w_2 values, indicated a net offshore transport for both wave conditions.

4.2 Sediment Transport

The equilibrium sediment concentration, C_{eq}, was used as a source term in the advection and diffusion model to solve for the sediment concentration at each time step (Pender & Karunarathna, 2013). The equilibrium sediment concentrations were calculated from one of three sediment transport formulations available in XBeach (i.e., Soulsby-Van Rijn model, Van Thiel-Van Rijn model, and Van Rijn model). The advection velocity introduces short wave non-linearity into the sediment transport computations through the advection velocity. The advection velocity was used in the advection and diffusion model to calculate the depth-averaged sediment concentration, which was used to compute the sediment transport rates at each time step, given by

$$q_t = C_s U_{reps} - D_h h \frac{\partial c}{\partial x} - 1.6 C_s V_{magu} \frac{\partial z}{\partial x} \tag{4.2}$$

where C_s is the depth-averaged sediment concentration, U_{reps} is $U_E + U_a$, D_h is the sediment diffusion coefficient, V_{magu} is the Lagrangian transport velocity, and U_a is the advection velocity. The calibrating factor for wave asymmetry and wave skewness (w_1 and w_2) were increased from 0 to 1 at an interval of 0.1 to investigate the change in the sediment transport rate as a result of the increasing advection velocity as described in Figure 3.8. The expected sediment transport rate for wave conditions 1 and 2 is onshore and offshore, respectively as per the Dean *et al*. (1973) Heuristic model (the non-dimensionalized fall velocity), displayed in Table 3.2.

4.2.1 Soulsby-Van Rijn Model

An increase in the sediment transport rate in the onshore direction is due to the increase in the wave asymmetry calibrating factor (w_1) as the wave skewness calibrating factor

(w_2) remains at the default value of 0.1 and vice versa. Additionally, an equal increase in the wave asymmetry and wave skewness calibrating factor results in an increase of the sediment transport rate (in the onshore direction) that is responsible for accretion. Although the magnitude of onshore sediment transport increases in all three cases of calibration, the magnitude of sediment transport varies as a function of the calibration case, sediment transport model, and wave conditions. The time-averaged sediment transport rate for both wave conditions with the increasing w_1 relative to w_2, increasing w_2 relative to w_1, and increasing w_1 and w_2 is displayed in Figure 4.4. The change in the sediment transport rate as a function of the w_1, w_2 and calibration case 3 are shown with the coloured lines.

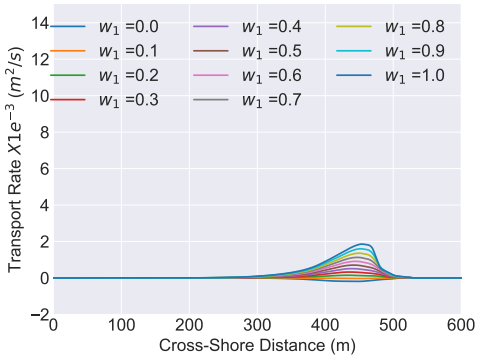

(a) $H_s = 1m$

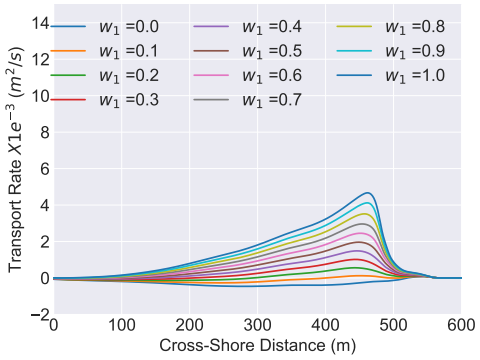

(b) $H_s = 3m$

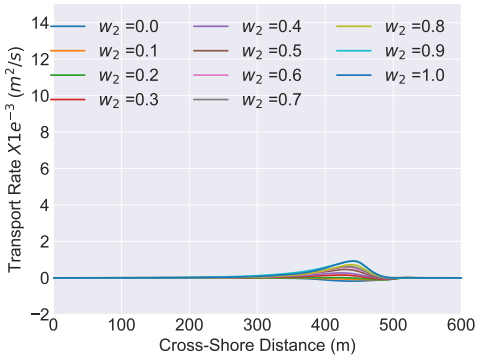

(c) $H_s = 1m$

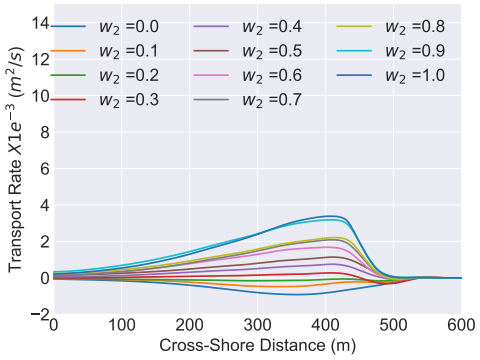

(d) $H_s = 3m$

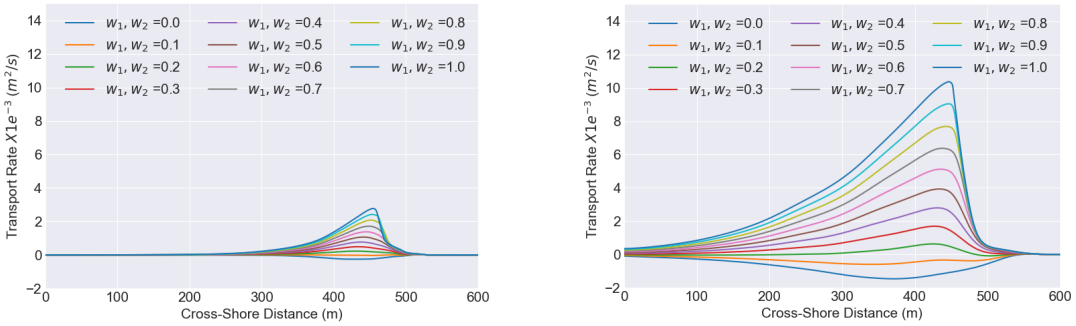

(e) $H_s = 1m$ **(f)** $H_s = 3m$

Figure 4.4. The change in sediment transport rate for the cross-shore domain computed using Soulsby-Van Rijn sediment transport model as a function of the wave conditions, and w_1, w_2 and calibration case 3 (w_1 and w_2 calibrating factors together). The range of colours represents the change in the w_1, w_2 and calibration case 3 values as indicated by the legend and described in Figure 3.8.

Figure 4.4 (a) and (b) display the resulting changes in the sediment transport rates with increasing w_1 values while leaving w_2 constant at the default values. Figure 4.4 (c) and (d) show the resulting changes in the sediment transport rates with increasing w_2 values while leaving w_1 constant at the default value. Figure 4.4 (c) and (d) show the resulting changes in the sediment transport rates with increasing values for calibration case 3. The Soulsby-Van Rijn sediment transport model predicts net offshore transport in the default mode for both wave conditions with default w_1, w_2 and calibration case 3 values of 0.1, as displayed in Figure 4.5. The results show that the sediment transport rates increase with the increasing w_1 value (while w_2 stays at a default value of 0.1, calibration case 1), increasing w_2 value (while w_1 stays at a default value of 0.1, calibration case 2), and increasing w_1 and w_2 values (calibration case 3). For the calibration case 1, w_1 value of less than 0.3 will produce net offshore sediment transport, and w_1 value of greater than 0.3 will produce a net onshore sediment transport, as shown in Figure 4.5 (a). For the w_2 and case 3 values less than 0.2 will produce net offshore sediment transport, while greater than 0.2 will produce a net onshore sediment transport, as shown in Figure 4.5 (b) and (c). The suitable w_1, w_2 or calibration case 3 values to use for long term morphological models, to maintain the equilibrium of net sediment transport rate, is 0.3 for w_1 and 0.2 for w_2 and calibration case 3.

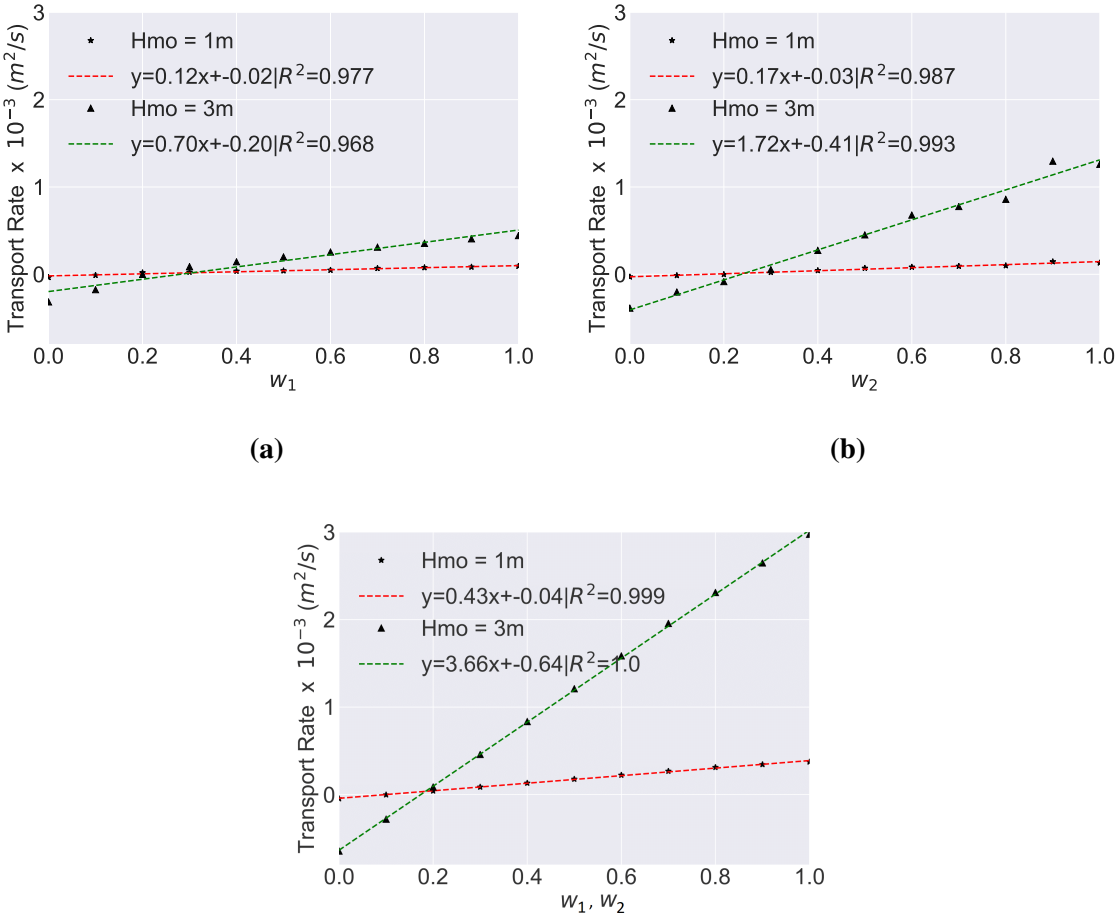

Figure 4.5. The change in net sediment transport rate for high and low energy waves ($H_s = 3$ m and $H_s = 1$ m, respectively) as a function of the w_1 shown in (a). The change in net sediment transport rate for high and low energy waves as a function of w_2 shown in (b). The change in net sediment transport rate for high and low energy waves ($H_s = 3$ m and $H_s = 1$ m, respectively) as a function of increasing w_1 and w_2 shown in (c).

4.2.2 Van Thiel-Van Rijn

The results show that the Van Thiel-Van Rijn sediment transport model has a similar response to the Soulsby-Van Rijn sediment transport model regarding the changes in the approaching wave energy and the calibration cases. The increase in wave energy and the increase in the calibration factor in calibration cases 1, 2, and 3 resulted an increase in the onshore sediment transport rate for the whole cross-shore domain. Figure 4.6 shows the time-averaged

sediment transport rate as a function of the two wave conditions and changing calibrating factors (indicated with the varying colours).

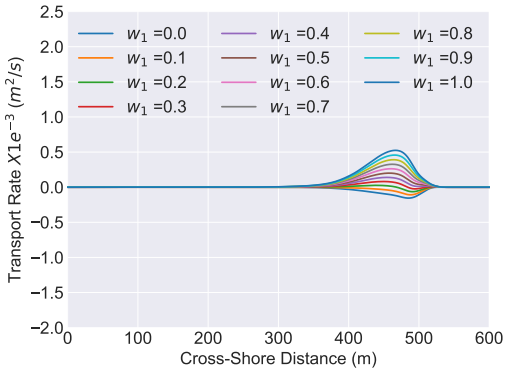

(a) $H_s = 1m$

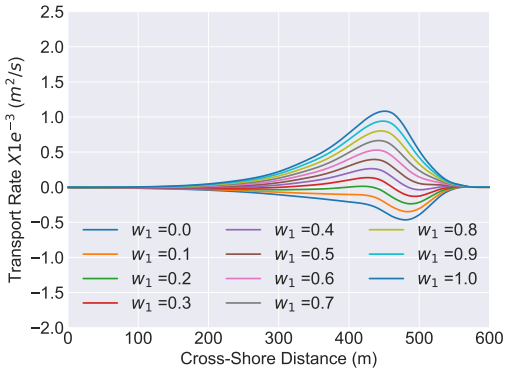

(b) $H_s = 3m$

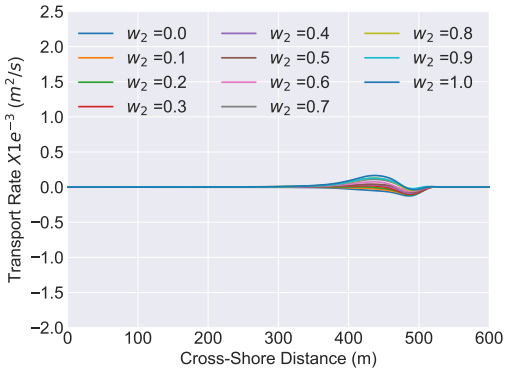

(c) $H_s = 1m$

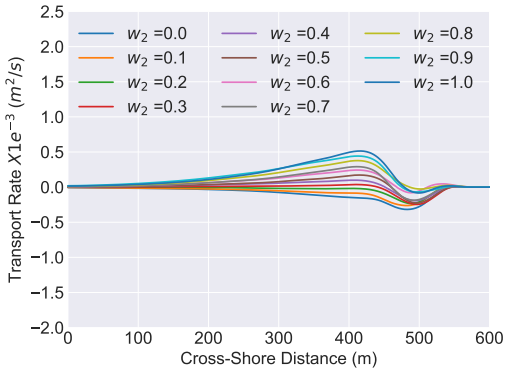

(d) $H_s = 3m$

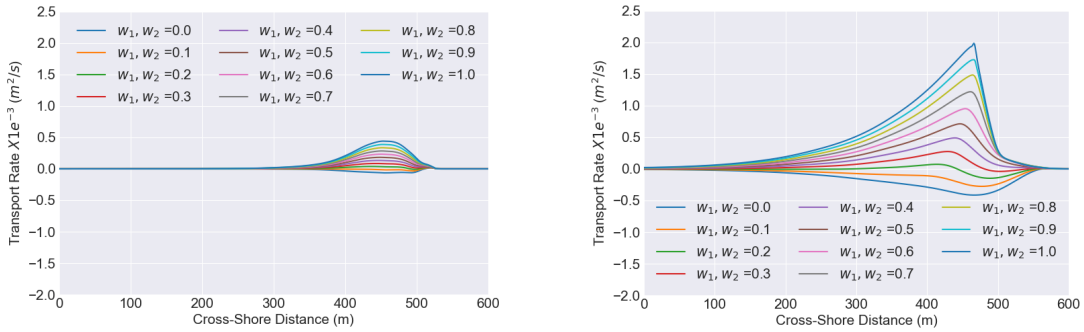

(e) $H_s = 1m$ **(f)** $H_s = 3m$

Figure 4.6. The change in sediment transport rate for the cross-shore domain computed using Van Thiel-Van Rijn sediment transport model as a function of the wave conditions, and w_1, w_2 and calibration case 3 (w_1 and w_2 calibrating factors together). The range of colours represents the change in the w_1, w_2 and calibration case 3 values as indicated by the legend and described in Figure 3.8.

Figure 4.6 (a) and (b) show the resulting changes in the sediment transport rates with increasing w_1 values while leaving w_2 constant at the default values. Figure 4.6 (c) and (d) show the resulting changes in the sediment transport rates with increasing w_2 values while leaving w_1 constant at the default value. Figure 4.6 (c) and (d) show the resulting changes in the sediment transport rates with increasing values in calibration case 3. The Van Thiel-Van Rijn sediment transport model, predicted net offshore sediment transport for the default w_1, w_2 and for calibration case 3 (w_1, w_2) values of 0.1, as displayed in Figure 4.7. The results show that a w_1 value (while w_2 stays at a default value of 0.1), and a w_2 value (while w_1 stays at a default value of 0.1) of less than 0,3 will produce net offshore sediment transport, while higher than 0,3 will produce a net onshore sediment transport, as shown in Figure 4.7 (a) and (b) respectively. Additionally, calibration case 3 values less than 0.2 will result in erosion and greater than 0.2 will result in accretion, as displayed in Figure 4.7 (c). The maintenance of the transport rate equilibrium is not due to the expected changes in the direction of net sediment transport rate for the given wave energy experienced by the beach face. However, it is due to the balance of onshore-offshore sediment transport at the given w_1, w_2 or calibration case 3 values. Therefore, these cross over values (w_1 and w_2 value of 0.3, and calibration

case 3 value of 0.2) can be applied to any wave condition in order to simulate onshore and offshore sediment transport.

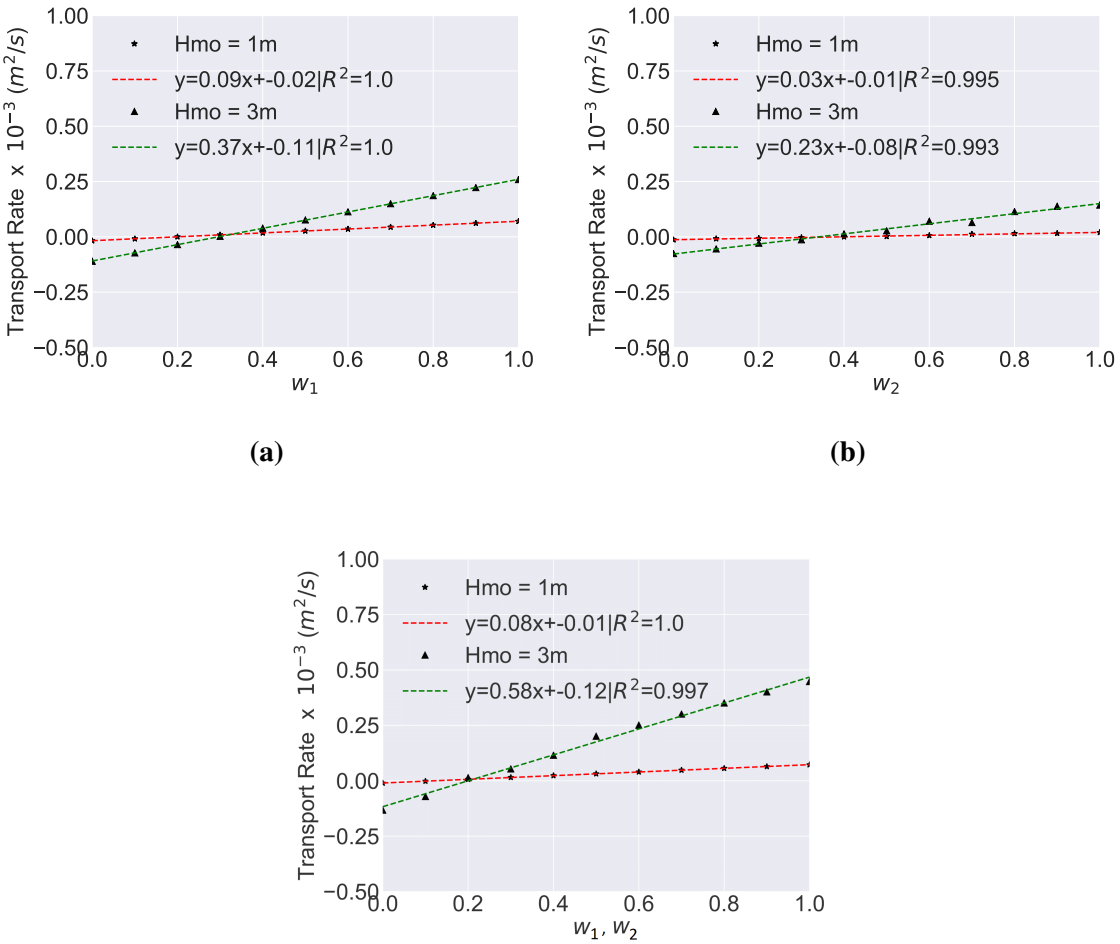

Figure 4.7. The change in net sediment transport rate for high and low energy waves ($H_s = 3$ m and $H_s = 1$ m, respectively) as a function of the w_1 shown in (a). The change in net sediment transport rate for high and low energy waves ($H_s = 3$ m and $H_s = 1$ m, respectively) as a function of w_2 shown in (b). The change in net sediment transport rate for high and low energy waves ($H_s = 3$ m and $H_s = 1$ m, respectively) as a function of increasing w_1 and w_2 shown in (c).

4.2.3 Van Rijn Model

The sediment transport rate computed by the Van Rijn sediment transport model increased as a result of the increasing w_1 value (while w_2 stays at a default value of 0.1, calibration

case 1) and increasing w_2 value (while w_1 stays at a default value of 0.1, calibration case 2). Additionally, an increase in calibration case 3 resulted in an increase of the sediment transport rate that is responsible for accretion. The results show that in comparison to the Soulsby-Van Rijn sediment transport model and Van Thiel-Van Rijn sediment transport models, the change in the w_2 relative to w_1 does not result in a significant enough change to produce an net onshore sediment transport rate, as shown Figure 4.8. However, increasing w_1 value relative to w_2 and an increase in calibration case 3 does result in a net onshore sediment transport rate at w_1, w_2, and calibration case 3 values higher than those obtained for the Soulsby-Van Rijn sediment transport model and Van Thiel-Van Rijn sediment transport model.

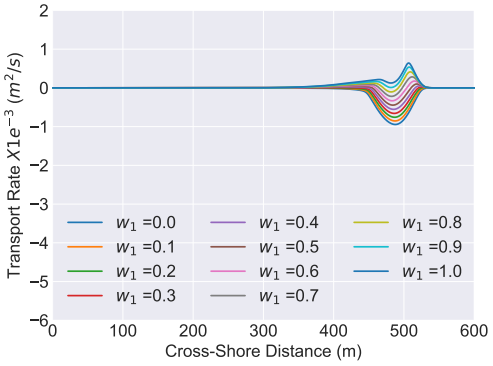

(a) $H_s = 1m$

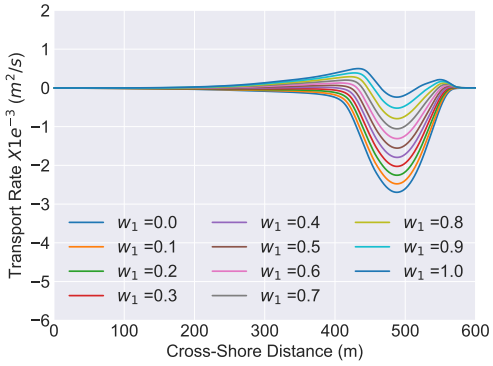

(b) $H_s = 3m$

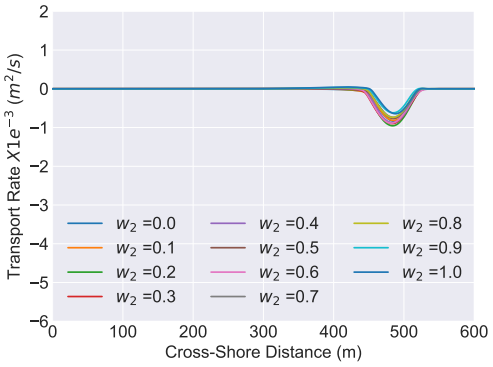

(c) $H_s = 1m$

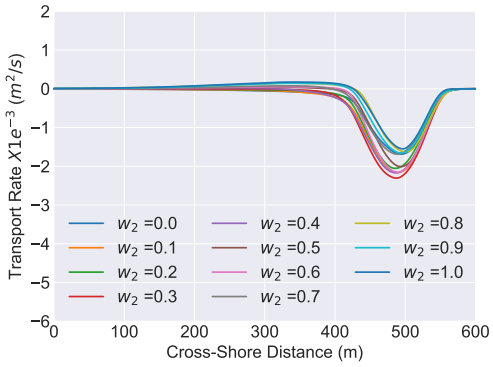

(d) $H_s = 3m$

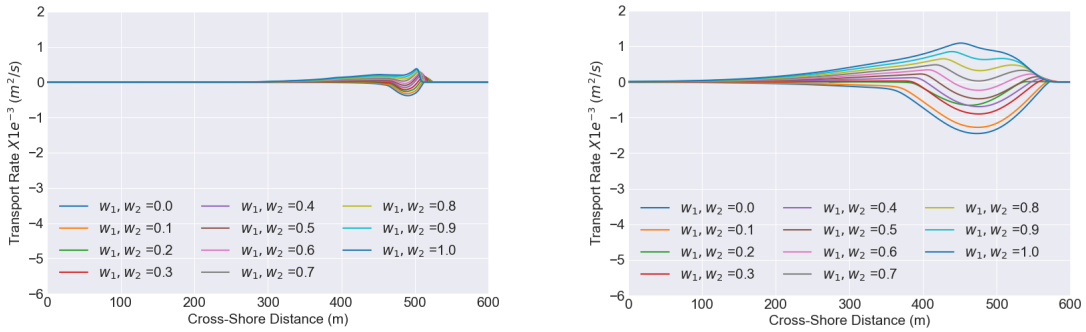

(e) $H_s = 1m$ **(f)** $H_s = 3m$

Figure 4.8. The change in sediment transport rate for the cross-shore domain computed using Van Rijn (1993) sediment transport model as a function of the wave conditions, and w_1, w_2 and calibration case 3 (w_1 and w_2 calibrating factors together). The range of colours represents the change in the w_1, w_2 and calibration case 3 values as indicated by the legend and described in Figure 3.8.

Figure 4.8 (a) and (b) show the resulting changes in the sediment transport rates with increasing w_1 values while leaving w_2 constant at the default values. Figure 4.8 (c) and (d) show the resulting changes in the sediment transport rates with increasing w_2 values while leaving w_1 constant at the default value. Figure 4.8 (c) and (d) show the resulting changes in the sediment transport rates with increasing values for calibration case 3. The Van Rijn (1993) sediment transport models predict net offshore for both wave conditions with the default w_1, w_2 and calibration case 3 values of 0.1, as displayed in Figure 4.9. The w_1 values less than 0,9 will produce net offshore sediment transport, while higher than 0,9 will produce a net onshore sediment transport, as shown in Figure 4.8 (a). Figure 4.8 (b) displays that the w_2 parameter does not change the direction of the sediment transport, as it was varied from 0 to 1 at an interval of 0.1 as described in Figure 3.8. Using the best-fit line, it was evident that w_2 will have to be 1.75 for H_s of 1m and 1.19 for H_s of 3m in order to reach a net-zero sediment transport rate. These w_2 values lie outside of the recommended maximum w_1 and w_2 values by XBeach. However, calibration case 3 values greater than 0.5 will result in accretion, and less than 0.5 will result in erosion, as displayed in Figure 4.8 (c).

This sediment transport model could not produce a net onshore sediment transport for both wave conditions with varying w_2. Therefore, the suitable w_1, and calibration case 3 to use for long term morphological models to maintain the equilibrium of net sediment transport rate (due to the balance of the offshore and onshore sediment movement) is 0.9 and 0.5, respectively.

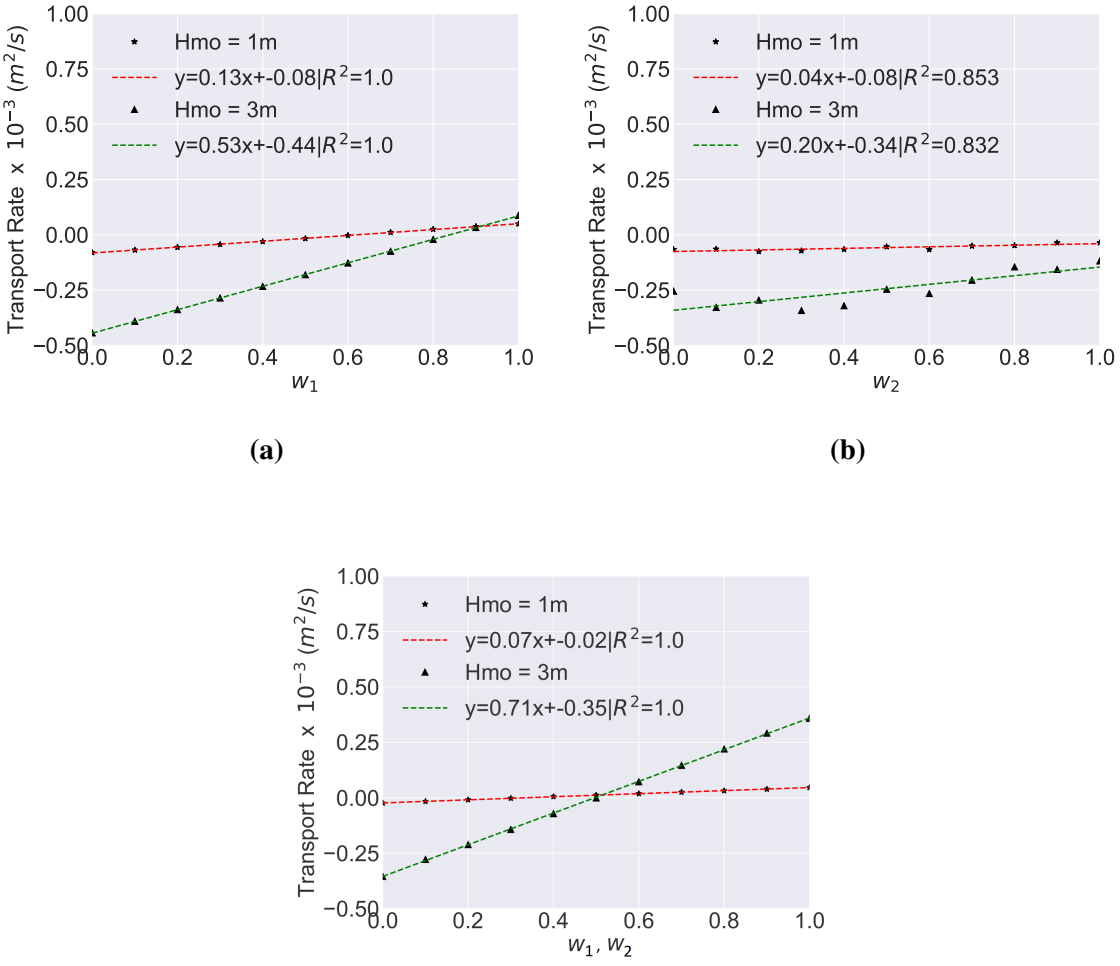

Figure 4.9. The change in net sediment transport rate for high and low energy waves ($H_s = 3$ m and $H_s = 1$ m, respectively) as a function of the w_1 shown in (a). The change in net sediment transport rate for high and low energy waves ($H_s = 3$ m and $H_s = 1$ m, respectively) as a function of w_2 shown in (b). The change in net sediment transport rate for high and low energy waves ($H_s = 3$ m and $H_s = 1$ m, respectively) as a function of increasing w_1 and w_2 shown in (c).

4.3 General Summary

The 3 cases explored showed that the sediment transport rates increased with increasing w_1 relative to w_2 (calibration case 1), increasing w_2 relative to w_1 (calibration case 2), and increasing w_1 and w_2 (calibration case 3). The point at which the sediment transport rate changes direction is different per calibration case, wave condition and sediment transport rate. Figure 4.10 shows the change in the sediment transport rate experienced in w_1 and w_2 space.

In summary, none of the sediment transport models available in XBeach have a calibrating parameter that will directly allow the calibration of these models, which will affect the sediment transport rates calculated. However, the w_1, w_2 or calibration case 3 parameters enable the calibration of the short wave asymmetry and wave skewness in the advection velocity used in the computation of the sediment transport rate. Figures 4.5, 4.7, and 4.9 show that varying the w_1 relative to w_2 values (calibration case 1), w_2 relative w_1 values (calibration case 2), and varying w_1 and w_2 (calibration case 3) produces significant net onshore or offshore sediment transport. To use any of the sediment transport models discussed to generate the beach volume and shoreline evolution data required to develop a simplified volumetric model, the w_1 and w_2 values must vary as a function of the approaching wave energy. This is essential in reproducing realistic sediment transport within the nearshore and offshore zone (up to the closure depth).

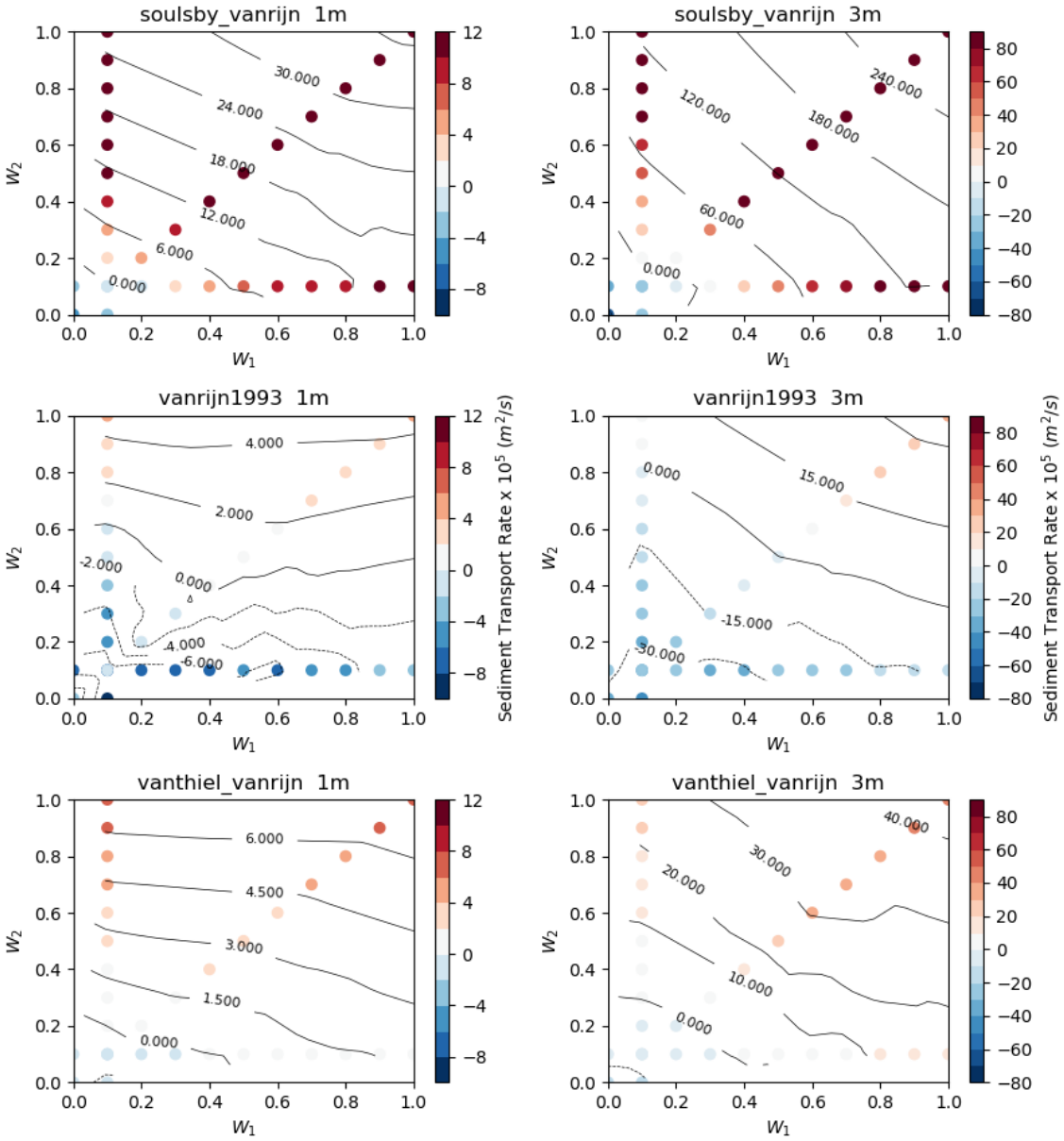

Figure 4.10. The three cases of wave asymmetry and wave skewness calibrating coefficient colour-mapped to the resulting net sediment transport experienced as a function of the wave condition and sediment transport model. Positive sediment transport rate is an accretion case while negative is an erosive case. The contours show the gradient of the sediment transport rate as a function of the calibration case.

CHAPTER 5: CONCLUSION AND RECOMMENDATIONS

5.1 Conclusion

The advection velocity (used in the advection-diffusion model in XBeach) was used to calculate the depth-averaged sediment concentration. It is a function of the representative velocity (U_{rms}), wave asymmetry, and wave skewness each calibrated by factors w_1 and w_2 respectively. The sensitivity of the sediment transport rate to the change in the advection velocity, and separately varying the wave asymmetry and wave skewness calibrating factors (w_1, w_2) was investigated in this study. Furthermore, the sensitivity of the sediment transport formulations available in XBeach were investigated with respect to the independently varying wave asymmetry and wave skewness calibrating factors. Accretive and erosive events were defined using the Dean's heuristic model (Dean *et al.*, 1973), given by

$$\Omega = \frac{H_s}{wT_P} \tag{5.1}$$

where Ω is non-dimensionalized fall velocity, Hs is significant wave height (m), w is sediment fall velocity (m/s), and Tp is wave period (s). Conditions where $\Omega > 3,2$ will result in an erosive case and $\Omega < 3,2$ will result in an accretive case. The nine-year wave data obtained from the waverider buoy, offshore of the Durban harbour, was used to select realistic wave conditions. The wave condition selection was dependent on the Dean's heuristic model.

This study also investigated the sensitivity of the flow velocity and advection velocity to the wave asymmetry and wave skewness calibrating factors (w_1, w_2). It was shown that the advection velocity increased with calibrating case 1, calibrating case 2 and calibrating case 3. Although the wave asymmetry or wave skewness calibrating factors (w_1, w_2) don't

have a direct influence on the flow velocity, the difference of the flow velocity and advection velocity was used to calculate the sediment transport rate.

The Soulsby-Van Rijn, Van Thiel-Van Rijn, and Van Rijn models were the sediment transport formulations investigated in this study. The sediment transport models in XBeach were investigated with wave conditions chosen using the dimensionless fall velocity. The dimensionless fall velocity was used to predict accretive and erosive events, as discussed in Section 2.3.2.

5.1.1 XBeach Cross-Shore Capability

The parametric study showed that for a single set of model parameters XBeach could not predict onshore sediment transport. Hence, the model needs to be calibrated to simulate accretive cases separately to erosive cases.

The Soulsby-Van Rijn model was the first sediment transport formulation investigated in this study. The sediment transport rate computed using this model increased as the wave asymmetry calibrating factor (w_1) increased while leaving w_2 constant at the default values, wave skewness calibrating factor (w_2) increased while leaving w_1 constant at the default values, and wave skewness calibrating factor (w_2) increased together with the wave asymmetry calibrating factor (w_1). For low values of w_1, w_2 and calibration case 3, the predicted net sediment transport rate is in the offshore direction for both high and low wave conditions. However, as the calibrating factors are increased, the sediment transport rate changes direction for both wave conditions, as discussed in Section 4.2.1. The wave asymmetry and wave skewness calibrating factors that balanced the onshore and offshore sediment transport was found to be 0.2 for all three sediment transport models investigated.

The Van Thiel-Van Rijn model was the second sediment transport model investigated. This sediment transport model is an adaptation of the Soulsby-Van Rijn model with the drag coefficient removed and the critical velocity computed in two parts. Namely critical velocity for currents and waves (Shields, 1936; Komar & Miller, 1975). The sediment transport rate

computed from the Van Thiel-Van Rijn model increased as the wave asymmetry calibrating factor (w_1) increased while leaving w_2 constant at the default values, wave skewness calibrating factor (w_2) increased while leaving w_1 constant at the default values, and wave skewness calibrating factor (w_2) increased together with the wave asymmetry calibrating factor (w_1). However, for the default value of the calibrating factors, the sediment transport rate for both high and low energy wave conditions was in the offshore direction. The wave asymmetry and wave skewness calibrating factors that balanced the onshore and offshore sediment transport was found to be 0.3 for calibration case 1 and case 2, and 0.2 for calibration case 3.

Finally, the Van Rijn model was the last sediment transport formulation investigated. This model calculated the sediment concentration in the water column as suspended sediment concentration, as discussed in section 2.5.2. Additionally, this model calculated the bed-load transport as a direct function of the mobility number due to waves and currents, sediment characteristics, and an excess sediment mobility number. Therefore, the calibrating factors only affected the magnitude and direction of the suspended sediment transport, as the bed-load transport was calculated by the sediment transport model itself. On the contrary, the suspended sediment concentration was calculated by the sediment transport model and used in the advection-diffusion model to calculate the depth-averaged sediment concentration. In this study, it was found that this sediment transport model can only reach a balance between onshore and offshore sediment transport as a function of the wave asymmetry calibrating factor (w_1) of 0.9, and the wave asymmetry and wave skewness calibrating factor (calibration case 3) of 0.5.

In summary, it can be concluded that the sediment transport rates are heavily influenced by the wave asymmetry and wave skewness calibrating factors (w_1 and w_2, respectively). In order to simulate realistic shoreline evolution and beach volume changes using XBeach, the wave asymmetry and wave skewness calibrating factors must be varied as a function of wave conditions, and sediment transport model used.

5.2 Recommendations

This section discusses the cross-shore sediment transport modeling capacity of XBeach and recommends the most suitable parameters to be used for the calibration of the sediment transport rate in the cross-shore direction. Additionally, recommendations are given for further research on the methods to be used for the development of a function that will improve the efficiency of the calibrating parameters used in XBeach, which will result in a more realistic sediment transport rate for a given wave condition.

5.2.1 Application of Short Wave Non-linearities calibrating Factors

None of the sediment transport models were able to produce onshore sediment transport under low wave energy and offshore sediment transport under high wave energy. These simulations were run under fixed model parameters that describe wave asymmetry and wave skewness effects. However, the calibrating factors investigated in this study can be adjusted in-order to predict accretion and erosion. The wave asymmetry and wave skewness calibrating factors that balance the onshore and offshore sediment transport are found to vary with the sediment transport model used, as discussed in Section 4.2 and summarized in Section 5.1.1. This can be used in the long term analysis of equilibrium cross-shore profiles, by using the calibrating factors obtained from a lookup table developed for a specific site, based on the average slope of the beach and the sediment size making up the beach. It must be noted that there is an interdependence between the incorporation of wave non-linearities and the sediment transport rate computation, where a better parametrization of the wave non-linearities will result in more realistic sediment transport and morphological changes.

5.2.2 Improving Cross-Shore Sediment and Morphological Modeling

In order to use the wave asymmetry and wave skewness calibrating factors realistically, they need to be a function of the incoming wave energy and sediment transport model used. Currently, the calibrating factors don't change as a function of the approaching wave

energy. Therefore, a relationship needs to be developed between the calibrating factors, and the wave energy and sediment transport model used. Wave flume data could be used to develop this empirical relationship. This relationship can thereby be incorporated into XBeach to produce more realistic shoreline evolution and beach profile changes because XBeach is an open-source software. The wave energy experienced by a coastal area changes at different time (on an hourly, daily, seasonal and yearly basis) and spatial scales. Therefore, using process-based models such as XBeach for long term simulations is not feasible as the computational demand is high. However, once the effect of the calibrating factors on erosion and accretion is addressed, XBeach can be used to generate the data required to develop a simple volumetric shoreline model for long term simulations that can be used to explore climate change and its effects on shoreline evolution.

Currently, the only way to run long term simulations is with one-line models or wave reduction models (Olij, 2015; Roelvink D, 2018). An example of a line model is the ShorelineS (Roelvink D, 2018). ShorelineS is capable of addressing non-linearities in the shoreline that arise due to high-wave angles. However, such models are limited to a particular contour and often do not incorporate both cross-shore and alongshore transport. Line models that do incorporate both alongshore and cross-shore sediment transport, combine the cross-shore and alongshore sediment transport at two different time scales (Vitousek *et al.*, 2017). The shortcoming of wave reduction models is wave sequencing and the decision on which morphological factors use (Olij, 2015).

A better approach to predicting long-term shoreline change is using a volumetric approach. However, this requires an understanding of the relationship between beach sand volume and profile shape, as well as the ability to relate it to the wave energy experienced by the coastal area. These fundamental relationships are not site-specific, have global applications for simulating shoreline behaviour, and aid in coastal engineering design. To explore long term changes experienced at any given coastal area due to the changing wave climates (which can be a result of climate change) the development of a simple model that takes into account

both the cross-shore and alongshore sediment transport is essential. This can be achieved by developing a simple volumetric shoreline model that incorporates both alongshore and cross-shore transport at different spatial and time scales, which will be less computationally demanding. Therefore, using the newly developed model, longer wave sequences and climate change effects can be explored in long term simulations.

REFERENCES

Airy, G., 1845. Tides and waves. In: Encyclopaedia metropolitana 5, 241.

Allan, J. C., Komar, P. D., 2003. A dynamic revetment and artificial dune for shore protection. In: Coastal Engineering 2002: Solving Coastal Conundrums. World Scientific, pp. 2044–2056.

Andrews, D., McIntyre, M., 1978. An exact theory of nonlinear waves on a lagrangian-mean flow. Journal of fluid Mechanics 89 (4), 609–646.

Battjes, J., 2001. Short waves (lecture notes ct4320). Delft University of Technology.

Battjes, J. A., 1975. Surf similarity. In: Coastal Engineering 1974. pp. 466–480.

Boechat Albernaz, M., Ruessink, G., Jagers, B., Kleinhans, M., 2019. Effects of wave orbital velocity parameterization on nearshore sediment transport and decadal morphodynamics. Journal of Marine Science and Engineering 7 (6), 188.

Bolle, A., Mercelis, P., Roelvink, D., Haerens, P., Trouw, K., 2011. Application and validation of xbeach for three different field sites. Coastal Engineering Proceedings 1 (32), 40.

Bosboom, J., Stive, M. J., 2012. Coastal dynamics I: lectures notes CIE4305. Delft University of Technology.

Clavero, M., Folgueras, P., Diaz-Carrasco, P., Ortega-Sanchez, M., Losada, M. A., 2018. A similarity parameter for breakwaters: the modified iribarren number. Coastal Engineering Proceedings (36), 28–28.

Corbella, S., Stretch, D., 2012a. Coastal defences on the kwazulu-natal coast of south africa: a review with particular reference to geotextiles. Journal of the South African Institution of Civil Engineering 54 (2), 55–64.

Corbella, S., Stretch, D., 2012b. Decadal trends in beach morphology on the east coast of south africa and likely causative factors. Natural Hazards and Earth System Sciences 12 (8), 2515–2527.

Corbella, S., Stretch, D. D., 2012c. Shoreline recovery from storms on the east coast of southern africa. Natural Hazards and Earth System Sciences 12 (1), 11–22.

Corey, A. T., 1949. Influence of shape on the fall velocity of sand grains. Ph.D. thesis, Colorado Agricultural and Mechanical College.

Dally, W. R., Dean, R. G., 1984. Suspended sediment transport and beach profile evolution. Journal of waterway, port, coastal, and ocean engineering 110 (1), 15–33.

Dean, R. G., 1991. Equilibrium beach profiles: characteristics and applications. Journal of coastal research, 53–84.

Dean, R. G., Dalrymple, R. A., 2004. Coastal processes with engineering applications. Cambridge University Press.

Dean, R. G., *et al.*, 1973. Heuristic models of sand transport in the surf zone. In: First Australian Conference on Coastal Engineering, 1973: Engineering Dynamics of the Coastal Zone. Institution of Engineers, Australia, p. 215.

Deigaard, R., *et al.*, 1992. Mechanics of coastal sediment transport. Vol. 3. World scientific publishing company.

Drake, T. G., Calantoni, J., 2001. Discrete particle model for sheet flow sediment transport in the nearshore. Journal of Geophysical Research: Oceans 106 (C9), 19859–19868.

EMS, 2007-2011. Technical Survey Report, Monthly Beach Monitoring Durban North, KwaZulu-Natal. Environmental Mapping and Surveying, P.O. Box 201155, Durban North, KwaZulu-Natal, 4016.

Fenton, J. D., 1985. A fifth-order stokes theory for steady waves. Journal of waterway, port, coastal, and ocean engineering 111 (2), 216–234.

Fernández-Mora, A., Calvete, D., Falqués, A., de Swart, H. E., 2015. Onshore sandbar migration in the surf zone: New insights into the wave-induced sediment transport mechanisms. Geophysical research letters 42 (8), 2869–2877.

Galappatti, G., Vreugdenhil, C., 1985. A depth-integrated model for suspended sediment transport. Journal of Hydraulic Research 23 (4), 359–377.

Grasso, F., Michallet, H., Barthélemy, E., 2011. Sediment transport associated with morphological beach changes forced by irregular asymmetric, skewed waves. Journal of Geophysical Research: Oceans 116 (C3).

Holman, R., Sallenger Jr, A., 1993. Sand bar generation: a discussion of the duck experiment series. Journal of Coastal Research, 76–92.

Hughes, M. G., Masselink, G., Brander, R. W., 1997. Flow velocity and sediment transport in the swash zone of a steep beach. Marine Geology 138 (1-2), 91–103.

Jara, M., González, M., Medina, R., 2015. Shoreline evolution model from a dynamic equilibrium beach profile. Coastal Engineering 99, 1–14.

Jeffreys, H., 1925. On the formation of water waves by wind. Proceedings of the Royal Society of London. Series A, Containing Papers of a Mathematical and Physical Character 107 (742), 189–206.

Kamphuis, J. W., 2010. Introduction to coastal engineering and management. Advanced Series on Ocean Engineering 30, 437.

Kemp, P., 1975. Wave asymmetry in the nearshore zone and breaker area. Nearshore sediment dynamics and sedimentation, 47–67.

Komar, P. D., Miller, M. C., 1975. On the comparison between the threshold of sediment motion under waves and unidirectional currents with a discussion of the practical evaluation of the threshold: Reply. Journal of Sedimentary Research 45 (1).

Lemos, C., Floc'h, F., Yates, M. L., Le Dantec, N., Marieu, V., Hamon, K., Cuq, V., Suanez, S. S., Delacourt, C., 2017. Equilibrium modeling of the beach profile on a macrotidal embayed beach. In: Aagaard, T., Deigaard, R., Fuhrman, D. (Eds.), Coastal Dynamics 2017. No. Paper No. 057 in Proceedings of Coastal Dynamics 2017. Helsingor, Denmark, pp. 760–771.
URL https://hal.archives-ouvertes.fr/hal-01580926

Longuet-Higgins, M. S., Stewart, R., 1964. Radiation stresses in water waves; a physical discussion, with applications. In: Deep Sea Research and Oceanographic Abstracts. Vol. 11. Elsevier, pp. 529–562.

Masselink, G., Hughes, M., Knight, J., 2014. Introduction to coastal processes and geomorphology. Routledge.

Mather, A. A., 2012. The risks, management and adaptation to sea level rise and coastal erosion along the southern and eastern african coastline. Ph.D. thesis, University of KwaZulu-Natal, 238 Mazisi Kunene Rd, Glenwood, Durban, 4041.

Mlche, R., 1944. Mouvements ondulatoirs des mers en profondeur constante on decroissant. Annals des Points et Chausses, 1U, 25–78.

Montes, S., 1998. Hydraulics of open channel flow. American Society of Civil Engineers, Baltimore, MD (US).

Olij, D. J. C., 2015. Wave climate reduction for medium term process based morphodynamic simulations. Master's thesis, Delft University of Technology, Mekelweg 5, 2628 CD Delft, Netherlands.

Pender, D., Karunarathna, H., 2013. A statistical-process based approach for modelling beach profile variability. Coastal Engineering 81, 19–29.

Pringle, J. J., 2015. On weather and waves : applications to coastal engineering. PhD dissertation, University of KwaZulu-Natal.

Rocha, M., Silva, P., Michallet, H., Abreu, T., Moura, D., Fortes, J., 2013. Parameterizations of wave nonlinearity from local wave parameters: a comparison with field data. Journal of Coastal Research 65 (sp1), 374–379.

Roelvink, D., 2011. A guide to modeling coastal morphology. Vol. 12. world scientific.

Roelvink, D., Reniers, A., Van Dongeren, A., De Vries, J. V. T., McCall, R., Lescinski, J., 2009. Modelling storm impacts on beaches, dunes and barrier islands. Coastal engineering 56 (11-12), 1133–1152.

Roelvink, D., Reniers, A., Van Dongeren, A., Van Thiel de Vries, J., Lescinski, J., McCall, R., 2010. Xbeach model description and manual. Unesco-IHE Institute for Water Education, Deltares and Delft University of Tecnhology. Report June 21, 2010.

Roelvink, J., 1993. Dissipation in random wave groups incident on a beach. Coastal Engineering 19 (1-2), 127–150.

Roelvink, J., 2003. Implementation of roller model, draft delft3d manual. Delft Hydraulics Institute. The Netherlands.

Roelvink D, Huisman B, E. A., 2018. Efficient modelling of complex coastal evolution at monthly to century time scales. Sixth International Conference on Estuaries and Coasts.

Rosati, J. D., 2005. Concepts in sediment budgets. Journal of Coastal Research, 307–322.

Ruessink, B., Miles, J., Feddersen, F., Guza, R., Elgar, S., 2001. Modeling the alongshore current on barred beaches. Journal of Geophysical Research: Oceans 106 (C10), 22451–22463.

Ruessink, B., Ramaekers, G., Van Rijn, L., 2012. On the parameterization of the free-stream non-linear wave orbital motion in nearshore morphodynamic models. Coastal Engineering 65, 56–63.

Sato, S., 1993. Sand transport under grouping waves. In: Coastal Engineering 1992. Coastal Engineering 1992, pp. 2411–2423.

Schwartz, L., Fenton, J., 1982. Strongly nonlinear waves. Annual review of fluid mechanics 14 (1), 39–60.

Shields, A., 1936. Anwendung der aehnlichkeitsmechanik und der turbulenzforschung auf die geschiebebewegung. PhD Thesis Technical University Berlin.

Sorensen, R. M., 2005. Basic coastal engineering. Vol. 10. Springer Science & Business Media.

Soulsby, R., 1997a. Dynamics of marine sands: a manual for practical applications. Thomas Telford.

Soulsby, R., 1997b. Dynamics of marine sands: a manual for practical applications. Thomas Telford.

Thornton, E., Humiston, R., Birkemeier, W., 1996. Bar/trough generation on a natural beach. Journal of Geophysical Research: Oceans 101 (C5), 12097–12110.

Türker, U., Kabdaşlı, M., 2007. Verification of sediment transport rate parameter on cross-shore sediment transport analysis. Ocean engineering 34 (8-9), 1096–1103.

Van Rijn, L. C., 1984. Sediment transport, part iii: bed forms and alluvial roughness. Journal of hydraulic engineering 110 (12), 1733–1754.

Van Rijn, L. C., 2007. Unified view of sediment transport by currents and waves. i: Initiation of motion, bed roughness, and bed-load transport. Journal of Hydraulic engineering 133 (6), 649–667.

Van Rijn, L. C., *et al.*, 1990. Principles of fluid flow and surface waves in rivers, estuaries, seas and oceans. Vol. 12. Aqua Publications Amsterdam, The Netherlands.

Van Rijn, L. C., *et al.*, 1993. Principles of sediment transport in rivers, estuaries and coastal seas. Vol. 1006. Aqua publications Amsterdam.

Van Thiel de Vries, J., Van de Graaff, J., Raubenheimer, B., Reniers, A., Stive, M., 2007. Modeling inner surf hydrodynamics during storm surges. In: Coastal Engineering 2006: (In 5 Volumes). World Scientific, pp. 896–908.

Van Thiel de Vries, J. S. M., 2009. Dune erosion during storm surges. Ph.D. thesis, Delft Unversity of Technology.

Vitousek, S., Barnard, P. L., Limber, P., Erikson, L., Cole, B., 2017. A model integrating longshore and cross-shore processes for predicting long-term shoreline response to climate change. Journal of Geophysical Research: Earth Surface 122 (4), 782–806.

Vousdoukas, M. I., Ferreira, Ó., Almeida, L. P., Pacheco, A., 2012. Toward reliable storm-hazard forecasts: Xbeach calibration and its potential application in an operational early-warning system. Ocean Dynamics 62 (7), 1001–1015.

Vreugdenhil, C. B., 2013. Numerical methods for shallow-water flow. Vol. 13. Springer Science & Business Media.

Walstra, D., Roelvink, J., Groeneweg, J., 2001. Calculation of wave-driven currents in a 3d mean flow model. In: Coastal Engineering 2000. Coastal Engineering 2000, pp. 1050–1063.

Wells, C. P., 2015. Modelling sand bypass schemes on the kwazulu-natal coastline. Master's thesis, University of KwaZulu-Natal, 238 Mazisi Kunene Rd, Glenwood, Durban, 4041.

Wright, J., Colling, A., Park, D., 1999. Waves, tides and shallow-water processes. Vol. 4. Gulf Professional Publishing.

Yu, X., Hsu, T.-J., Hanes, D. M., 2010. Sediment transport under wave groups: Relative importance between nonlinear waveshape and nonlinear boundary layer streaming. Journal of Geophysical Research: Oceans 115 (C2).

APPENDIX A: MODEL INPUT PARAMETERS AND VALUES

Table A.1 XBeach Model Input

Physical Processes		
	wavemodel	surfbeat
Turn on sediment transport	sedtrans	1
morphology	morphology	1
avalanching	avalanching	1
groundwater flow	gwflow	1
Grid Parameters		
Number of computational cell corners in x-direction	nx	628
Number of computational cell corners in y-direction	ny	0
Bathymetry is specified positive down (1) or positive up (-1)	posdwn	-1
Name of the input bathymetry file	depfile	bed.dep
Name of the file containing x-coordinates of the calculation grid	xfile	x.grd
Name of the file containing y-coordinates of the calculation grid	yfile	y.grd
Number of computational cells in z-direction	nz	20
Lower directional limit (angle w.r.t computational x-axis)	thetamin	90
Higher directional limit (angle w.r.t computational x-axis)	thetamax	360
Directional resolution	dtheta	10
Model Time Parameters		
Stop time of simulation, in morphological time	tstop	3800

Physical Constants		
Density of water	rho	1025
Gravitational acceleration	g	9.81
Wave Boundary Condition Parameters		
New wave boundary condition type	wbctype	parametric
Name of spectrum file	bcfile	jonsp.txt
Wave-Spectrum Boundary Condition Parameters		
Switch to enable random seed for instat = jons, swan or vardens boundary conditions	random	0
Duration of wave spectrum at offshore boundary, in morphological time	rt	1800
Flow Boundary Condition Parameters		
Switch for seaward flow boundary	front	abs_1d
Switch for lateral boundary at ny+1	left	wall
Switch for lateral boundary at 0	right	wall
Switch for boundary at bay side	back	abs_1d
Tide Boundary Conditions		
Inital water level	zs0	0
Wave Breaking Parameters		
Type of breaker formulation	break	roelvink2
Breaker parameter in baldock or roelvink formulation	gamma	0.78
Flow Parameters		
Bed friction formulation	bedfriction	manning
Bed friction coefficient	bedfriccoef	0.02
Sediment Transport Parameters		
Equilibrium sediment concentration formulation	form	**Varies**
Calibration factor time averaged flows due to wave skewness	facSk	**Varies**

Calibration factor time averaged flows due to wave asymmetry	facAs	**Varies**
Calibration factor for suspensions transports	sus	1
Calibration factor for bed transports	bed	1
Modify the magnitude of the sediment transport based on the bed slope, uses facsl	bdslpeffmag	roelvink_bed
Bed Composition Parameters		
Porosity	por	0.4
D50 grain diameters for all sediment classses	D50	0.000355
Morphology Parameters		
Morphological acceleration factor	morfac	1
Critical avalanching slope under water (dz/dx and dz/dy)	wetslp	.3
Critical avalanching slope above water (dz/dx and dz/dy)	dryslp	1
Output Variables		
Start time of output, in morphological time	tstart	0
Interval time of global output	tintg	1
Interval time of mean, var, max, min output	tintm	1800
Number of global output variables (as specified by user)	nglobalvar	14
Bed level	zb	
Asymmetry of short waves	As	
Skewness of short waves	Sk	
Orbital velocity	urms	
Reflected velocity at bnds in u-points	ur	
Representative flow velocity for sediment advection and diffusion, x-component	urepb	
Representative flow velocity for sediment advection and diffusion, x-component	ureps	

Wave energy	E	
Hrms wave height based on instantaneous wave energy	H	
Eulerian velocity in u-points, x-component	ueu	
Bed sediment transport for each sediment class (excluding pores), x-component	Subg	
Sediment concentration integrated over bed load and suspended and for all sediment grains	cctot	
Depth-averaged bed equilibrium concentration for each sediment class	ceqbg	
Depth-averaged suspended equilibrium concentration for each sediment class	ceqsg	
Number of mean, min, max, var output variables	nmeanvar	4
Sediment transport integrated over bed load and suspended and for all sediment grains, x-component	Sutot	
Sediment concentration integrated over bed load and suspended and for all sediment grains	cctot	
Depth-averaged bed equilibrium concentration for each sediment class	ceqbg	
Depth-averaged suspended equilibrium concentration for each sediment class	ceqsg	

NonDimensionalization of Advection Velocity

$u^a = x_1 \times \frac{\pi H_{rms}}{T_p sinh(2kh))}$

where:

$x_1 = (-w_1 \times As + w_2 \times Sk)$

where H_{rms} is Root mean square wave height, T_p is Wave period, k is wavenumber, h is Water depth, u^a is the advection velocity, u^E is current flow velocity, and w_1 and w_2 are the wave asymmetry and skewness calibrating factors applied to the wave skewness (Sk) and asymmetry (As) respectively.

x_1 has no dimension.Hence, only the U_{orb} has to be non-dimensionalised.

$U_{orb} = \frac{\pi H_{rms}}{T_p sinh(2(\frac{2\pi}{L}))h))}$

where the dimensions of each parameter are:

$H_{rms} = m \ \ [meters]$
$T_p = s \ \ [seconds]$
$h = m \ \ [meters]$
$L = m \ \ [meters]$

The nondimentionalisation of the U_{orb} is as follows:
$U_{orb} = \frac{\pi[m]}{[s]sinh(2(\frac{2\pi}{[m]}))[m]))}$

$U_{orb} = \frac{\pi[m]}{[s]sinh(4\pi)}$

$$U_{orb} \times \frac{T_p}{H_s} = \frac{\pi H_{rms}}{T_p sinh(4\pi)} \times \frac{T_p}{H_s}$$

$$U_{orb} \times \frac{T_p}{H_s} = \frac{\pi [m]}{[s] sinh(4\pi)} \times \frac{[s]}{[m]}$$

$$U_{orb} \times \frac{T_p}{H_s} = \frac{\pi}{sinh(4\pi)}$$

Therefore, the nondimentionalised advection velocity is:

$$u_a \times \frac{T_p}{H_s} = x_1 \times \frac{\pi}{sinh(4\pi)}$$

APPENDIX B: SEDIMENT CHARACTERISTICS DATA

Table B.1 The percentage sediment retained in each sieve size for samples from Mgeni River to Umhlanga (2009-2011).

D_{50}	Date							
	2/1/2009	**8/1/2009**	**12/1/2009**	**2/1/2010**	**4/1/2010**	**8/1/2010**	**12/1/2010**	**4/1/2011**
4mm	1.379310345	0.862068966	1.293103448	0.603448276	1.293103448	0.344827586	0.689655172	1.293103448
2mm	10.0862069	11.89655172	10	5.086206897	11.63793103	3.793103448	9.137931034	6.724137931
1.41mm	12.24137931	15	12.24137931	9.310344828	12.32758621	5.25862069	12.4137931	6.637931034
1mm	14.39655172	13.79310345	14.39655172	14.74137931	13.01724138	9.137931034	15.94827586	10.34482759
710um	16.29310345	14.22413793	16.37931034	20.25862069	14.39655172	15.51724138	18.44827586	16.37931034
500um	14.65517241	14.9137931	14.65517241	20	15.60344828	19.74137931	16.46551724	18.62068966
355um	12.84482759	13.10344828	12.84482759	14.56896552	13.70689655	21.29310345	12.4137931	21.03448276
250um	13.10344828	11.89655172	13.10344828	11.55172414	13.01724138	19.05172414	8.965517241	14.31034483
180um	4.310344828	3.793103448	4.310344828	3.620689655	4.482758621	5.431034483	2.75862069	3.965517241
125um	0.775862069	0.517241379	0.775862069	0.517241379	0.603448276	0.689655172	0.517241379	0.517241379
90um	0.172413793	0.086206897	0.172413793	0.086206897	0.172413793	0.172413793	0.086206897	0.172413793
65um	0	0	0	0	0.086206897	0	0	0.086206897
mud	0	0	0	0	0	0	0	0

Table B.2 The first, second, third quantile (Q_1, Q_2, and Q_3 respectively) and 95^{th} percentile of the average percentage sediment retained in each sieve size for samples taken from the coastline stretching from the Mgeni River to Umhlanga in the KZN coastline.

D_{50}	**Percentile**			
	0.25	**0.5**	**0.75**	**0.95**
4mm	0.668103448	1.077586207	1.293103448	1.349137931
2mm	6.314655173	9.568965517	10.47413793	11.80603448
1.41mm	8.64224138	12.24137931	12.34913793	14.09482759
1mm	12.34913793	14.09482759	14.48275862	15.52586207
710um	15.23706897	16.3362069	16.89655172	19.625
500um	14.84913793	16.03448276	18.90086207	19.90948276
355um	12.84482759	13.40517242	16.18534483	21.20258621
250um	11.81034483	13.06034483	13.40517242	17.39224138
180um	3.75	4.137931035	4.353448276	5.099137931
125um	0.517241379	0.560344828	0.711206896	0.775862069
90um	0.086206897	0.172413793	0.172413793	0.172413793
65um	0	0	0.021551724	0.086206897

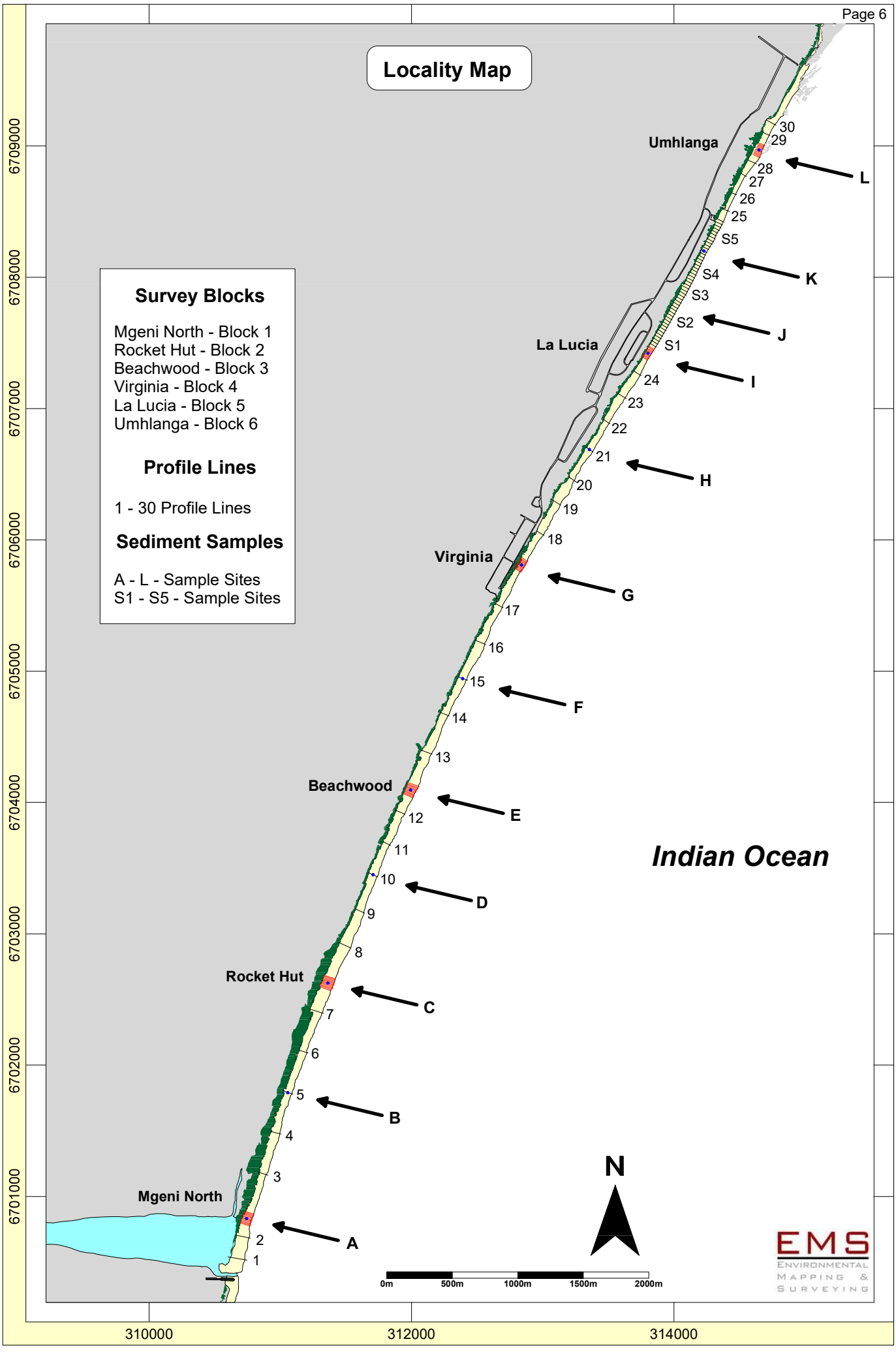
Locality Map
Survey Blocks
Mgeni North - Block 1
Rocket Hut - Block 2
Beachwood - Block 3
Virginia - Block 4
La Lucia - Block 5
Umhlanga - Block 6
Profile Lines
1 - 30 Profile Lines
Sediment Samples
A - L - Sample Sites
S1 - S5 - Sample Sites
Umhlanga
La Lucia
Virginia
Beachwood
Rocket Hut
Mgeni North
Indian Ocean
N
0m
500m
1000m
1500m
2000m
EMS
Environmental Mapping & Surveying
6709000
6708000
6707000
6706000
6705000
6704000
6703000
6702000
6701000
310000
312000
314000